Science of the Total Environment 1002 (2025) 180584

Contents lists available at ScienceDirect

Science of the Total Environment

journal homepage: www.elsevier.com/locate/scitotenv

Research Paper

The hidden consequences of agricultural development: Soil degradation and pesticide contamination in the South American Pampa

Amaury Bardelle [a,*], Renaldo Gastineau [b], Floriane Guillevic [c], Anthony Foucher [a], Pierre-Alexis Chaboche [a], José Antonio Corcho-Alvarado [d], Stefan Röllin [d], Guillermo Chalar [e], Pierre Sabatier [b], Marcos Tassano [f,g], Nathalie Cottin [b], Rosalie Vandromme [h], Olivier Cerdan [h], Christine Alewell [c], Olivier Evrard [a]

[a] Laboratoire des Sciences du Climat et de l'Environnement (LSCE-IPSL), Université Paris-Saclay, UMR 8212 (CEA-CNRS-UVSQ), Gif-sur-Yvette, France
[b] EDYTEM, Université Savoie Mont Blanc, CNRS, Bâtiment Pôle Montagne, 5 bd de la mer Caspienne, Le Bourget du Lac, France
[c] Environmental Geosciences, University of Basel, Basel, Switzerland
[d] Nuclear Chemistry Division, Spiez Laboratory, Federal Office for Civil Protection, Austrasse, Spiez, Switzerland
[e] Instituto de Ecología y Ciencias Ambientales, Sección Limnología, Facultad de Ciencias, Universidad de la República, Montevideo, Uruguay
[f] Laboratorio de Radioquímica, Área de Radiofarmacia, Centro de Investigaciones Nucleares. Facultad de Ciencias, Universidad de la República, Montevideo, Uruguay
[g] Instituto de Investigación Una Salud. Facultad de Ciencias, Universidad de la República, Montevideo, Uruguay
[h] Risk and Prevention Division, Bureau de Recherches Géologiques et Minières (BRGM), Orléans, France

HIGHLIGHTS

- Four phases of agricultural development and their impacts identified since 1945.
- Expansion of agriculture on natural landscapes increased sediment fluxes.
- Erosion was minimal under no-till with pasture rotation and maximal without rotation.
- DDT resurgence in 1990s/2000s resulting from remobilisation of contaminated sediment.
- Need for continuous monitoring of sediment and pollutant dynamics in the Pampa.

GRAPHICAL ABSTRACT

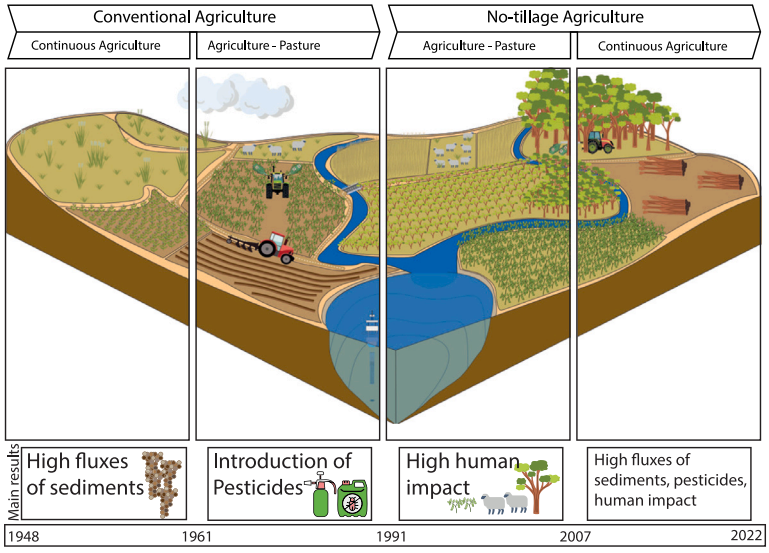

ARTICLE INFO

Keywords:
Sediment dynamics
Pesticide contamination

ABSTRACT

Agricultural expansion has led to an acceleration of soil erosion and sediment dynamics in South America in general and in the Pampa biome in particular. This region is a hotspot of land-use and land-cover changes and

* Corresponding author.
E-mail address: amaury.bardelle@icloud.com (A. Bardelle).

https://doi.org/10.1016/j.scitotenv.2025.180584
Received 3 May 2025; Received in revised form 19 September 2025; Accepted 20 September 2025
Available online 3 October 2025

Agricultural expansion
Radionuclide dating
Farming practice changes

was marked by important and rapid shifts in farming practices. However, the environmental consequences of these changes remain under-documented.

To address this lack, the current research uniquely reconstructed sediment fluxes since the 1950s in the Pampa region in Uruguay from a sediment archive collected in a dam reservoir inaugurated in 1945. This core was analysed following a multi-proxy approach and fluxes of key pesticides were reconstructed since the 1950s. Results revealed that while early agricultural phases included widespread pesticide use, their impact remained limited due to the limited size of cultivated areas. A transitional period to no-tillage farming and pasture rotation first reduced sediment delivery. Nevertheless, afterwards, large-scale land conversion, combined with intensive pesticide application, has led to another episode of acceleration in soil erosion and an increase in sediment fluxes, largely decoupled from the precipitation variability alone. Notably, a resurgence of the banned DDT pesticide was observed suggesting the possible remobilisation of DDT originating from past applications. These findings provide long-term insights into the environmental consequences of the changes in land-use, land-cover and farming practices since the mid-twentieth century in a relatively understudied region and highlight the need for continued monitoring and for the implementation of measures to mitigate soil erosion and pesticide contamination in the Pampa region.

1. Introduction

South America has experienced significant landscape transformations driven by the expansion of agriculture (pasture, cropland, tree plantations) over the last 70 years. This expansion took place at the expense of natural ecosystems. Since 1985, pasture, cropland, and forest plantation areas have increased by 23%, 160%, and 288%, respectively, often replacing natural vegetation, including natural tree cover (−16% in South America) and natural grasslands (−26% in Southern Brazil) (Oliveira et al., 2017; Zalles et al., 2021). This shift has led to widespread soil degradation, a loss of biodiversity, and natural habitat destruction (Zurbriggen et al., 2020).

The Pampa biome, which is a temperate grassland ecosystem primarily located in Uruguay, southern Brazil and central eastern Argentina, has recently emerged as one of the global hotspots of land-use change (Baeza et al., 2022). These changes threaten soil and water resources as well as biodiversity in a biome that stores large quantities of carbon and supports unique ecosystems (Andrade et al., 2023). The Brazilian Pampa covers slightly over 2% of Brazil's surface area, but it holds about 9% of its total biodiversity (Andrade et al., 2023). Despite the importance of this biome in terms of biodiversity and soil carbon storage, 80% of Uruguayan soils located in the Pampa region were already affected by degradation in 2008 (Chiappe et al., 2008).

The agricultural land expansion and the changes in farming practices from a conventional tillage-based system to a no-tillage-based agriculture in Uruguay started in the 1990s, and they then accelerated in the early 2000s with the aim of reducing soil degradation and erosion. This change has been made possible following the decrease in the cost of herbicides along with the introduction of genetically modified herbicide-resistant crops (Merotto et al., 2022). Accordingly, this shift from a tillage-based to a no-tillage agriculture created a heavy reliance of farmers on the use of pesticides in general, and on glyphosate in particular. Locally, continuous soybean monoculture replaced the traditional crop-pasture rotation, reducing biodiversity and altering weed populations (Merotto et al., 2022). Regionally, the expansion of genetically modified crops, especially glyphosate-resistant soybean, led to a surge in herbicide use, causing ecological shifts such as the expansion of herbicide-resistant weeds, which now represents a major threat for agriculture in Uruguay (Merotto et al., 2022).

Locally, some studies have quantified soil redistribution rates in the region. For instance, Cabrera et al. (2023) reported median net erosion rates of 1.4 to 19.3 t ha^{-1} yr^{-1} in contrasting river basins (covering 19.8 to 171.1 km^2) in Uruguay. They used ^{137}Cs and excess lead-210 ($^{210}Pb_{ex}$) measurements to reconstruct soil losses over different periods and under contrasted land-uses at sites that started to be intensively cultivated before the 1960s. Furthermore, an average soil redistribution rate of 7 t ha^{-1} was found at sites characterised by extensive cattle ranching. Subsequently, soil losses and soil health degradation can lead to regional and basin-scale impacts. Indeed, nutrient-enriched runoff has been linked to toxic cyanobacteria blooms that have prevented water from meeting public health standards since 2010 (Kruk et al., 2023).

More generally, in addition to the increases in soil losses and sediment/nutrient transfers to water bodies, the use of pesticides in modern agriculture was shown to contaminate soil, water and the vegetation, and it was proved to be toxic for both biodiversity (Aktar et al., 2009) and human populations. Accordingly, Skidmore et al. (2023) demonstrated a statistically significant increase in paediatric leukaemia following soybean crop production expansion in the region, with an increased exposure of the populations to pesticides that may occur via the contamination of the water supply.

However, there is a lack of historical records to reconstruct these pesticide-related pressures. Moreover, few quantitative data are available for the period of agricultural expansion, since the mid-twentieth century, on the impact of the changes in land-use and in farming practices on the evolution of soil and water quality along with soil loss at the regional scale and for the period of agricultural expansion since the mid-twentieth century.

In this context, the objective of the current research is to understand how changes in land-use and agricultural practices, i.e. the shift from natural to anthropogenic landscapes, the transition from conventional to no-tillage farming, and the application of pesticides, may have impacted sediment transfers in the Pampa Biome region since the onset of modern agricultural development.

To this end, retrospective studies using reservoir sediment cores may provide a powerful means to reconstruct long-term environmental changes in the absence of continuous monitoring, as demonstrated by Foucher et al. (2023). These approaches have also been used to reconstruct contaminant and pesticide transfers across different contexts and timescales (Garcia-Rodrıguez et al., 2002).

In South America in general, and in the Pampa biome in particular, such reconstructions are associated with major challenges, including the limited number of lakes and reservoirs suitable for sediment coring operations. Additional parameters, such as the reservoir size, the extent of its drainage area, and the year of reservoir construction, must also be considered when selecting potential sampling sites.

Foucher et al. (2023) successfully identified a reservoir in Uruguay that meets these criteria and collected a sediment core to investigate the impacts of landscape modifications on sediment production. However, their analysis was restricted to the recent period comprised between 1990 and 2020 as they could not investigate earlier changes in land-use, land-cover and agricultural practices (i.e., tillage transition and increasing pesticide use).

To address this gap, the present study analysed a longer sediment core retrieved from the same site, the Rincón del Bonete reservoir, draining a 39,500 km^2 transnational catchment from Uruguay and Southernmost Brazil. This core, which reached the reservoir's bottom, is expected to cover the full period since the dam construction (i.e. 1945), allowing to reconstruct the impact of land-use and agricultural practices on sediment dynamics since World War II, which is almost unique

in this part of the world where limited historical archive/data have been made available to date. Furthermore, the originality of this study lies in the extensive multi-proxy analysis conducted to reconstruct sediment dynamics and relate this data to global and socio-economic trends. Among the analyses performed, a combination of radionuclides including plutonium isotopes were analysed and used to validate the chronology of the sediment core.

More specifically, the study's objectives were threefold: (1) to establish an accurate chronology of the sediment core and validate it, (2) to quantify sediment fluxes and compare them with historical phases of agricultural development in Uruguay, and (3) to reconstruct pesticide fluxes during the successive phases of agricultural expansion and outline their potential impacts on sediment transfers.

2. Materials and methods

2.1. Study site

The Rincón del Bonete catchment is transboundary with 9% of its surface area being located in Brazil and 91% in Uruguay. It is located within the Pampa biome, mainly in the central and northern regions of Uruguay (Fig. 1) with a geomorphology of hilly to rolling landscapes.

The Rincón del Bonete catchment has two major tributaries including Rio Tacuarembó and Rio Negro (Fig. 1). These two rivers drain very contrasting landscapes with distinct reliefs, geologies and soil types, reflecting the occurrence of different ecoregions (Arocena et al., 2022). On the one hand, the Rio Negro, in the western part of the river basin, drains a region characterised by the presence of mudstones and limestones that support the formation of Mollisols, dark soils, which are rich in organic matter, silt, and clay and that are mainly used for crop cultivation. In contrast, the Rio Tacuarembó drains a region mainly composed of Alfisols, underlied by sandstones, characterised by leached and weathered acidic soils with low organic matter content, showing the country's lowest fertility, or shallow sandy or coarser soils with rock outcrops and loose stones on the surface, predominantly used for forest plantations (Arocena et al., 2022).

Overall, land-use in the Rincón del Bonete catchment remained dominated by natural herbaceous vegetation (61%) in 2023. in addition, the catchment was also occupied with cropland cultivated using no-tillage practices (14%), forest plantations (11%), natural forests (5%), wetlands (4%), water bodies (3%) and non-vegetated areas (1%) (Fig. 1).

Furthermore, the Rincón del Bonete catchment drains into a reservoir whose surface area varies between 465–1495 km^2 (1140 km^2 in optimal conditions). Built in 1937 and inaugurated in 1945, this reservoir is used to generate electric power in Uruguay. Importantly, the Rincón del Bonete reservoir has never been emptied or dredged since its creation. This reservoir is the largest freshwater body in Uruguay (5 km^3 of water storage) with a ratio of 25–33 km^2 of drainage basin per km^2 of reservoir, thereby exceeding the storage capacity of the other reservoirs in the country, including the large Salto Grande and Palmar dams, with respective reservoir surfaces of 783 and 320 km^2 (World Lake Database - 2025).

The climate in Uruguay is considered as humid subtropical according to the Koppen Climate Classification (World Meteorological Organisation - Clasificación climática). Precipitation in the Rivera municipality, a meteorological station located in the Northern part of the catchment, amounted for an annual mean of 1525 mm yr^{-1} for the 1991–2020 period. The monthly precipitation is the lowest in June, July and August with 79 mm mth^{-1} on average. During the rest of the year, precipitation is higher and more constant with an average of 143 mm mth^{-1}. The month with the highest precipitation in the Rivera municipality is April, with an average of 180 mm for the 1991–2020 period (World Meteorological Organisation - Tablas estadísticas).

2.2. Data sources

Land-use was reconstructed in the investigated catchment using the set of maps provided by the MapBiomas network (MapBiomas Pampa) for the Pampa biome for the 1985–2022 period (Baeza et al., 2022). The river basin data were retrieved from the maps published for each year during this period. In the last version of MapBiomas, a distinction was made between permanent pasture and temporary crops. Permanent pastures were defined by MapBiomas as the "cultivation of perennial herbaceous forage species, that persist for more than one year", while temporary crops were defined as the "cultivation of annual herbaceous species that are planted and harvested within one year". Increase and decrease percentages were calculated following Eq. (1).

$$\text{Variation } (\%) = \left(\frac{\text{New value} - \text{Old Value}}{\text{Old value}}\right) \cdot 100 \quad (1)$$

Rainfall was reconstructed at the scale of the investigated river basin using the climate knowledge portal database (https://climateknowledgeportal.worldbank.org/) and the Climate Engine solution with TerraClimate precipitation calculations (https://app.climateengine.org). This database available at the catchment scale covers the period 1958–2023, at a monthly resolution. This dataset was chosen as is the longest that could be found over the river basin.

To compare the precipitation variations with the reconstructed fluxes of sediments obtained, the mean precipitation per month for each year was calculated. Periods of multiple years with higher precipitation than the calculated median for the whole sequence were also identified.

A 48 cm long sediment (22-BONETE-03) core was collected in December 2022 in the Rincón del Bonete reservoir (IGSN number: 10.58052/IEFOU002D) by local researchers using a Uwitec gravity corer available at the Universidad de la República (Montevideo, Uruguay) equipped with 90 mm PVC liners on a floating platform and by hammering. The sediment core was collected in the original Rio Negro river channel. This channel was identified with a sonar, at 2.5 km from the dam (Fig. 1, under 20 m water depth) to ensure a reconstruction of the complete sedimentation history since the dam creation.

2.3. Methodology

The analysis conducted, their resolution and the associated units were summarised in Table A.2. Readers can refer to this table for a fast and clear understanding of all the measurements carried out.

2.3.1. Particle size analysis

Particle size analysis was performed on fresh sediment at a centimetric resolution with a laser diffraction particle size analyser (Mastersizer 3000 with Hydro LV, Malvern Panalytical) in osmotic water on fresh sediment with sonic dispersion to minimise particle flocculation. Each sediment sample was analysed five times. The particle size distribution was measured in the range from 0.01 μm to 3500 μm, and the fraction indices D10, D50, D90 corresponding to the proportion of particles smaller than 10%, 50% and 90% were extracted. Besides sonic dispersion, no other treatment was conducted on the sediment.

2.3.2. Density analysis

Relative density of the sediment was recorded with a Computer Tomography scanner (CT-scan) every 0.625 mm. Images were recorded via a GE Discovery CT750 HD instrument available on the DOSEO platform (French Atomic Energy and Alternative Energy Commission, CEA Paris-Saclay, France). Relative density (grey values) measured with the CT scan were extracted from the reconstructed images via the Free software ImageJ.

Bulk density (ρ_b) was then measured on 8 samples of fresh sediment using a 1.7 cm^3 (V) acrylic cube. The cubes were filled with fresh sediment, the humid weight (m_{humid} in g) was reported, then oven-dried at 40 °C for 48 to 96 h, and the dry weight (m_{dry} in g) was finally

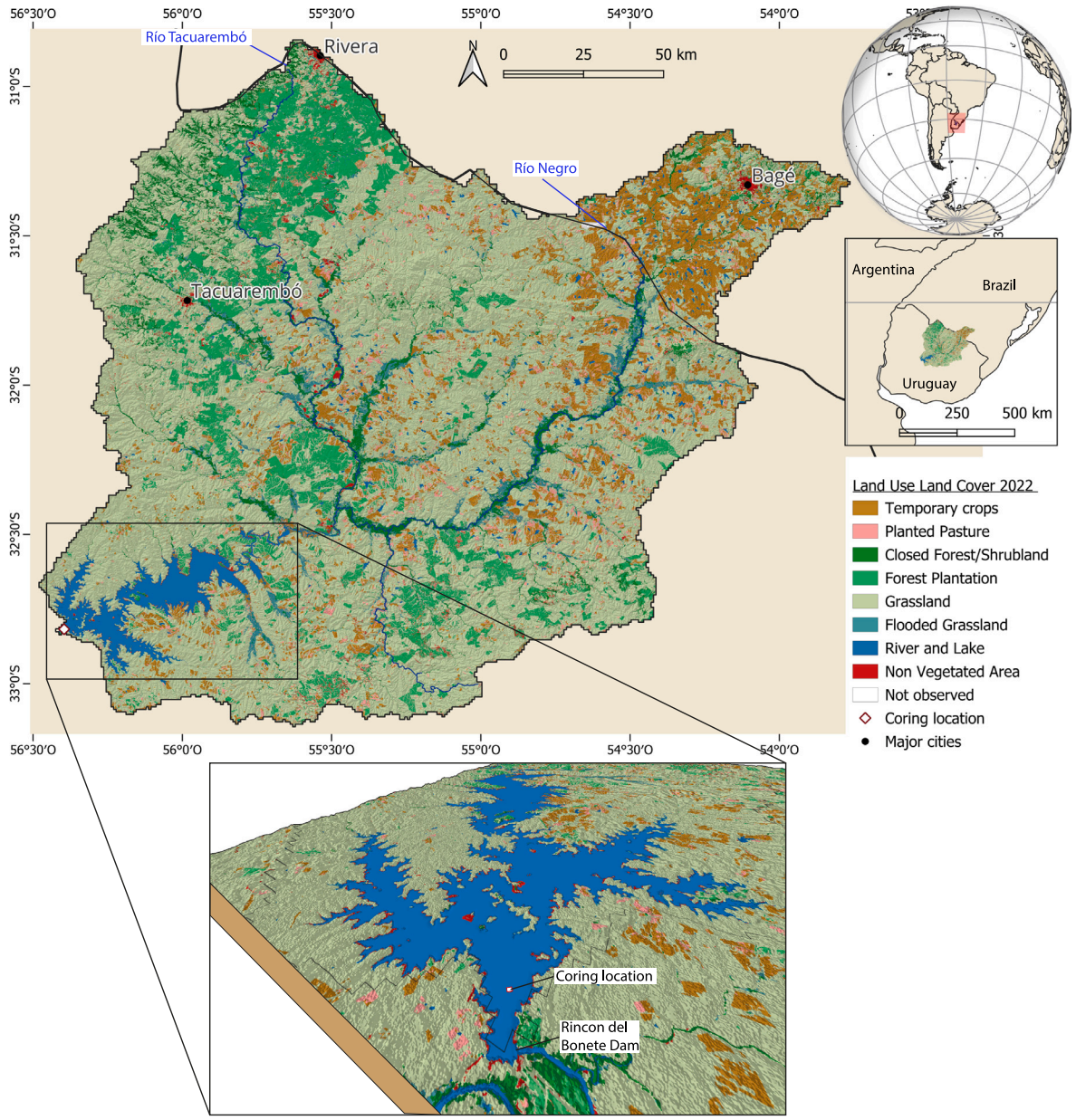

Fig. 1. Location of the Rincón del Bonete River basin in South America, coring location (S32° 49.072', W56° 24.008') and map of land-uses and covers in 2022 (MapBiomas Pampa), background map from OpenStreetMap.

measured. The bulk density (ρ_b in g cm^3) was calculated following Eq. (2).

$$\rho_b = \frac{m_{dry}}{V} \quad (2)$$

The mean values of the Ct scan relative density (grey values) over the samples were correlated to the bulk density, and density was reconstructed for the whole sequence following the procedure proposed by Foucher et al. (2023).

2.3.3. Organic matter analysis

One-half of the core was subsampled following depth increments of 1 cm. The sediment was dried at 40 °C for 48 h and ground before total organic carbon (TOC) concentration, nitrogen concentration (TN) measurements and stable C (δ^{13}C) isotope ratios were determined.

The %TOC, %TN and δ^{13}Corg contents were measured using an elemental analyser (Flash HT 2000) coupled to an isotope ratio mass spectrometer Advantage delta V via a conflow IV interface from Thermo Scientific. The EA-IRMS instrument was calibrated against two standards (i.e., EMAP2 and USGS24). Analytical precision and repeatability were assessed via the analysis of reference material (Low Organic Standard and High Organic Standard). In the current research, the mean uncertainties amounted to 0.01% for TN, 0.06% for TOC, 0.1‰ for δ^{13}C. The ^{13}C isotope content is expressed as δ^{13}C in against Pee Dee Belemnite (PDB). This is a standard reference for δ^{13}C, measured on shells of a species of belemnite from the Upper Cretaceous.

2.3.4. Gamma spectrometry analysis

Gamma spectrometry measurements were conducted on 1-cm layers of dried and ground sediment samples using a 'well' type HPGe detector (Canberra/Ortec®) available at the Modane underground laboratory, a subterranean low-background laboratory located within the Fréjus Road Tunnel, near Modane, France. This laboratory is shielded from cosmic radiation by 1700 m of rocks and is only equipped with very low activity materials and copper-lead shielded detectors to achieve ultra-low background in order to analyse low-radioactivity samples in

the best conditions. The activities of lead-210 in excess ($^{210}Pb_{ex}$) were calculated by subtracting the two Radium-226 daughters, Lead-214 (average count at 295.2 and 351.9 keV) and Bismuth-214 (609.3 keV), from the total ^{210}Pb activities detected at 46.5 keV. ^{137}Cs activities were measured at 662 keV and decay-corrected to the sampling date.

All measurements were corrected for background levels determined every two months and for detector and geometry efficiencies.

2.3.5. Plutonium analysis

Based on the vertical distribution of ^{137}Cs activities in the sediment core, 16 samples among those analysed in gamma spectrometry were selected for additional plutonium analyses (^{239}Pu, ^{240}Pu). Measurements were conducted at the Spiez Laboratory in Switzerland following the methodology established by Röllin et al. (2022). Pu isotopes were measured using ICP-MS and MC-ICP-MS after a series of purification and separation steps. The samples were fused, dissolved and filtered to remove silicates, and then Pu was extracted using TEVA, UTEVA, and DGA resins. The isotopes were then quantified using high-sensitivity ICP-MS techniques, correcting for interferences and validating the results with certified reference materials.

2.3.6. Pesticide analysis

A total of 16 pesticides and their metabolites (Table A.1), which were commonly reported in the literature for the Pampa region, were measured at EDYTEM Laboratory (Univ. Savoie Mont-Blanc, France) (Mañay et al., 2004; Palladino et al., 2023).

In order to conduct the pesticide analyses, the second half of the core collected as described above was sampled following depth increments of 2 cm from 0 to 20 cm and then following depth increments of 4 cm from 20 cm to 45 cm. This second set of samples was freeze-dried in an ALPHA 1–2 LD plus (CHRIST®) freeze dryer for 24 to 48 h, depending on the sample quantity available.

Pesticides were then extracted via the QuEChERS method; the Quick, Easy, Cheap, Effective, Rugged, and Safe extraction kit and method (Perestrelo et al., 2019). Pesticide concentrations were obtained via Gas and Liquid Chromatography coupled with Mass Spectrometry (GC–MS for Endosulfan, Chlopryrifos Ethyl, DDT,DDD, DDE, and Mirex and LC-MS/MS for S-Metolachlor, Simazine, Atrazine, Diruon, 2.4-D, Tebuconazole, Imidacloriprid and Friponil). Glyphosate and AMPA were analysed by a rapid LC-MS/MS method with a Polypore H+ column without derivatisation, with a good selectivity and sensitivity.

Once the concentration of pesticides was obtained (g g^{-1}), the equivalent in moles of pesticides (mol g^{-1}) was calculated by dividing each pesticide's concentration by its molar mass (g mol^{-1}).

Extensive research was conducted in the literature and multiple technical reports were analysed in order to obtain different information on the pesticides, such as their dates of first production/marketing and are described and used for interpretation in the results and discussion, Section 3.6.

2.3.7. Age model and sediment fluxes

Sediment core chronology was established using $^{210}Pb_{ex}$ activities measured in a set of 29 samples. The *serac* R package for ShortlivEd RAdionuclide Chronology (Bruel and Sabatier, 2020) was used for the establishment of the age model via the Constant Flux Constant Sedimentation (CF:CS) model. The age model was validated by identifying the transition from coarser particles to finer sediments at the base of the core, which was associated with the level of the Rio Negro paleochannel corresponding to the dam impoundment period (age model date 1948 ± 3 years, inauguration of the dam in December 1945). In addition, artificial radionuclides fallout (^{137}Cs, $^{240+239}$Pu activities, and the associated $^{240/239}$Pu ratios) from past nuclear weapon tests were used as an independent time-marker to validate the age model (Chaboche et al., 2022). The age-depth model was validated by radionuclide deposition chronology/pattern affecting South America, including the onset of global detection of nuclear test fallout in 1954, the peak of maximum fallout in the Southern Hemisphere in 1964–1965, and specific nuclear bomb signatures such as those associated with several French nuclear tests conducted in Polynesia between 1966–1974 (UNSCEAR 2008 Report).

Sediment fluxes (MAR, Mass Accumulation Rate, g cm^{-2} yr^{-1}) were reconstructed by multiplying SAR (cm yr^{-1}) obtained from the CF:CS age model with high-resolution densities calibrated from the CT scan values (g cm^{-3}); Eq. (3).

Mean fluxes of sediment were calculated based on the high frequency MAR records. The different values of MAR for each year were added and divided by the number of observations available for each year.

$$\text{MAR (g cm}^{-2}\text{ yr}^{-1}) = \text{ Sedimentation rate (cm yr}^{-1}) \cdot \text{ Density (g cm}^{-3}) \quad (3)$$

Pesticides fluxes were derived from the sediment fluxes. To this end, the moles of pesticides were converted into fluxes by multiplying the quantities of pesticides with the MAR (Eq. (4)).

$$\text{Fluxes of pesticides (mol cm}^{-2}\text{ yr}^{-1}) = \text{ Pesticides (mol g}^{-1}) \cdot \text{ MAR (g cm}^{-2}\text{ yr}^{-1}) \quad (4)$$

2.3.8. Statistical tests

The Mann–Kendall Test was applied to identify generally positive or negative (p-values < 0.5) trends in precipitation using the R package. The result of the test, 'tau', varies between −1 and 1; it is positive when the trend increases and negative when the trend decreases. In addition, the breaking point test (Hurtado et al., 2020) available in R (https://CRAN.R-project.org/package=BreakPoints) was performed to identify MAR shifts and to check whether their occurrence matched with contrasted phases of agricultural development as documented in the literature for Uruguay.

In order to identify when the data undergoes a significant change, a breakpoint test is performed on the data series. A breakpoint is validated when the *p*-value was sufficiently low (in the present case, *p*-value < 0.05). Three breakpoints are searched for in the MAR values to identify the four contrasting periods of sediment inputs identified in the literature (and described in Section 3.1). Each period has to represent at least three years, taking into account the uncertainty associated with the age model, for a complete period to be considered. Finally, the test is applied using the statistical methods established by Pettitt (1979) and Buishand (1982). The reason for choosing these two statistical methods is that, as Hurtado et al. (2020) demonstrated, they exhibit a high ability to reproduce the date of the breakpoints when they occurred in the middle of a time series, which is of interest here.

In order to compare and characterise the periods identified in the sediment fluxes with the breakpoint test, a series of tests is applied using the rstatix, Stats, PMCMRplus and FSA packages in R. First, the normality of the data is tested using a Shapiro–Wilk test. Then, a Kruskal–Wallis rank sum test, a non-parametric alternative to ANOVA, is applied to compare the medians across the periods identified in the sediment fluxes. Finally, a Dunn's post hoc test with the commonly used Bonferroni correction is applied for pairwise comparisons to specify which groups differed from each other.

3. Results and discussion

All the data produced during this study, the variable description and metadata are available on Zenodo (Physico-chemical properties of a sediment core collected in the Rincon del bonete dam reservoir, Uruguay to reconstruct environmental changes (1945--2023)).

3.1. Evolution of the land-use land-cover

MapBiomas data shows an overall prediction accuracy of 76%–79%, depending on the year under consideration (Baeza et al. (2022), MapBiomas - Methodology Collection 4). For the last collection released, a robust classification approach combining spectral and temporal data was applied to distinguish between pasture and cropland. Given their often similar appearance on satellite imagery, especially during certain growing stages, misclassification may occur. The methodology uses annual mosaics, phenological indicators, and post-classification temporal filters to reduce these potential misclassifications. These filters improve temporal consistency by penalising inter-annual land-use changes that are unlikely to occur in reality, ensuring that transitions reflect real dynamics. This data provided valuable insights into the reconstruction of agricultural expansion, deforestation, tree plantation, and changes in other human activities across the Pampa biome's ecosystems. The temporal resolution of the dataset is also well suited for tracking long-term patterns and assessing policy impacts on land use.

From 1985 to 2022, land-use changes in the Rincón del Bonete basin followed two main axes and mainly affected the natural grasslands. Forest plantations expanded in the northwestern and southeastern regions, while agriculture and pasture increased in the northeast (Fig. 2). The central part of the basin remained relatively intact. This expansion, originating from the Northern part of the river basin, in Brazil, spread southwards along the Río Negro, primarily targeting fertile Mollisol regions for farming and grazing. In parallel, forest plantations developed along the western Río Tacuarembó in Alfisol-dominated areas, where poor soil quality limited agricultural use (Arocena et al., 2022).

More specifically, forest plantations covered less than 1% of the catchment surface area in 1985. This proportion increased to more than 10% in 2022 (Fig. 2), an increase of 1573% in 37 years. Several periods of accelerated forest plantation are observed, such as those that took place between 1999 and 2005 (increase of 195%) and, more recently, between 2014 and 2019 (increase of 18% of the catchment area).

Permanent pastures increased by more than 169% from 1985 to 2022. 2018 is the year with the maximum area under pasture representing 4.6% of the river basin's area. This progression follows three rising periods (1995–2000, 2003–2005 and 2011–2014). Finally, a slowdown of this trend is observed since 2015 (Fig. 2).

Moreover, the area covered by temporary crops increased from 2.5% of the catchment area in 1985 to more than 10% in 2022. A steady increase is observed between 1985 and 2005, followed by a sharper rise until 2013. It then slows down again before re-accelerating from 2019 to 2022 (Fig. 2).

In parallel, the area occupied by natural grassland decreased by 25%, as it represented 83% of the Rincón del Bonete river basin surface in 1985 but only 63% in 2022. A strong period of reduction of the surfaces devoted to natural grasslands is observed in 2002–2005 (Fig. 2). These results are comparable with those found by Oliveira et al. (2017) in the nearby Brazilian Pampa. These authors found indeed that the area under natural pastures decreased by 26% since 1975. In parallel, cultivated forests and temporary crops were the land uses showing the highest growth between 1985–2005, particularly during the second half of this period, from 1995 to 2005.

Natural forests (mean 5.0%), wetlands (mean 3.3%), non-vegetated areas (mean 1.2%), as well as water surfaces (mean 3.0%) remained constant throughout the period (±1%–2%).

Based on the land-use and land-cover changes as well as historical records, four periods of agricultural development in Uruguay were identified and described. The first period, from the 1950s until the 1960s, was characterised by continuous cultivation with minimal technological advancements (Hudson et al., 1992). It was then followed by a second period, from the 1970s until the 1990s, marked by the adoption of extensive pesticide use, and the introduction of a crop-pasture rotation system (Merotto et al., 2022), however, most of the catchment area remained largely unexploited (90% of the river basin was then occupied by natural landscapes, i.e. shrublands, wetlands and grasslands), except for the Brazilian uppermost portion (Fig. 2).

From 1990 onwards, a transition occurred as the government voted a law, which granted tax exemptions and even subsidised forestry plantations to initiate and encourage the implementation of these technologically advanced farming techniques (Zurbriggen et al., 2020). A drastic expansion of the area of soybean was also observed, permitted in Uruguay by the authorisation of planting genetically modified soybean seeds and the land leasing law that encouraged short-term leases from 1996. This expansion was accompanied by a transition towards no-tillage agriculture (Garcia-Préchac et al., 2004). As shown by Derpsch et al. (2010), 32% of cropland was cultivated under no-tillage in 2000–2001 compared to 82% in 2006–2007). This third period, from the 1990s to 2002 initially maintained the crop-pasture rotation system, with the implementation of soil conservation practices (Zurbriggen et al., 2020). However, in the subsequent fourth period, from 2002 onwards, this system was abandoned in favour of continuous cultivation and double cultivation (i.e. the planting of two or more crops on the same plot and during the same year), consisting in an intensification of agricultural practices (Rizzo et al., 2021).

As shown in the literature (Hudson et al., 1992; Derpsch et al., 2010; Zurbriggen et al., 2020), changes in land-use and practices across the river basin were influenced by political shifts in the country.

3.2. Sediment analyses

The 22-BONETE-03 sequence is characterised by homogeneous fine brown-coloured sediment. No specific facies or layers could be visually observed when opening the core. However, the layer corresponding to the Rio Negro River channel deposits that took place before the dam impoundment can be visually observed at the base of the core, with the occurrence of coarser sand particles as well as vegetation debris.

Above this facies transition, the D10 index varies between 0.25 and 5.2 ± 1.2 μm along the core, whereas the D50 index varies between 7.0 and 25.2 ± 4.6 μm, and D90 varies between 45.0 and 179.8 ± 41.5 μm (Fig. 3).

Two minima in grain size values are observed, with D10 and D50 indices of 0.3 ± 0.009 μm and 7.1 ± 0.1 μm at 5 cm, and 0.25 ± 0.01 μm and 7.2 ± 0.3 μm at 10 cm, respectively. D90 amounted to 7.2 ± 2.9, and 46.1 ± 13.8 μm at 5 and 10 cm, respectively.

From grain size data as well, the results indicate that the sediment core exhibits a high degree of homogeneity.

TOC values varies from 2.8% at 12 cm to 4.9% at the bottom of the core (44–45 cm) above the pre-dam facies, with an average value of 3.2 ± 1% (Fig. 3). Three peaks are observed at 38, 32 and 10 cm, with values of 3.8%, 3.6%, and 3.7%, respectively. $\delta^{13}C$ remains stable throughout the core (from −18.8 to −22.6‰), except for two minima found at 30 and 11 cm depths, with values of −20.5 and −22.6‰, respectively.

$\delta^{13}C$ values observed in the sediment sequence reflect the type of plants that grew in soils eroded across the river basin and transported to the reservoir. Overbeck et al. (2007) found the coexistence of C_3 and C_4 plants in the Southern Brazilian grasslands of Rio Grande do Sul (in which the northernmost part of Rincón del Bonete river basin is located). Higher values of $\delta^{13}C$ around −16 to −10‰ correspond to the signature of C_4 plants, while lower values of $\delta^{13}C$, between −33 and −24‰ correspond to C_3 plants. This region was predicted to be covered by 50 to 70% of C_4 plants, with values of $\delta^{13}C$ around −20‰ by Powell and Still (2009). Bueno et al. (2021) found similar mean values between −19.73 ± 0.35‰ and −18.58 ± 0.55‰. They also found the same trends with a decrease of values in the uppermost layer with values of −23.26‰ and −23.53‰ , which are consistent with those values found in the core analysed in the current research.

The TOC/TN ratio varies between 7 and 11, with an average value of 9 ± 0.3. Overall, this parameter remains stable along the core,

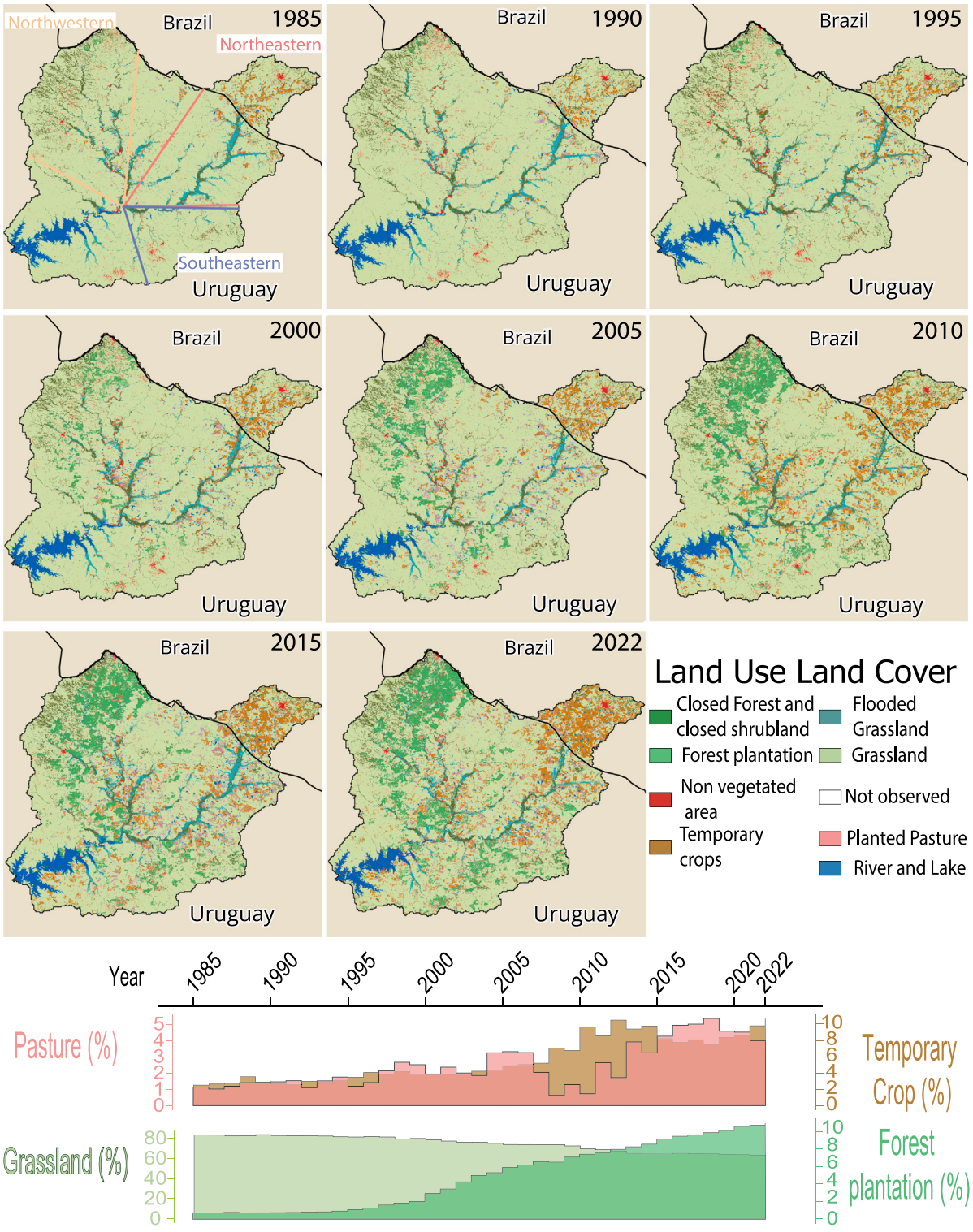

Fig. 2. Evolution of land-use and land-covers from 1985 to 2022 (MapBiomas Pampa) and representing area (in %) of pasture, grassland, temporary crop and forest plantation extracted from the MapBiomas dataset, background map from OpenStreetMap. The northwestern, southeastern and northeastern parts of the basin are shown for the 1985 map in light orange, red and blue.

following the same trends as TOC. The minimum value is observed at the top of the core and the maximum is found at 38 cm depth (with values of 7.2 and 10.9, respectively). The TOC/TN ratio shows the same trends as those observed for TOC, with peaks at 38, 30 and 11 cm depths, with respective values of 10.9, 10.9 and 9.5.

The analysis of the TOC/TN ratio provides insights into the provenance of the organic matter, categorised as allochthonous (originating from the catchment) or autochthonous (resulting from biological activity within the reservoir). Terrestrial plants, part of the allochthonous matter, generally show values of TOC/TN above 12 (Lamb et al., 2006)

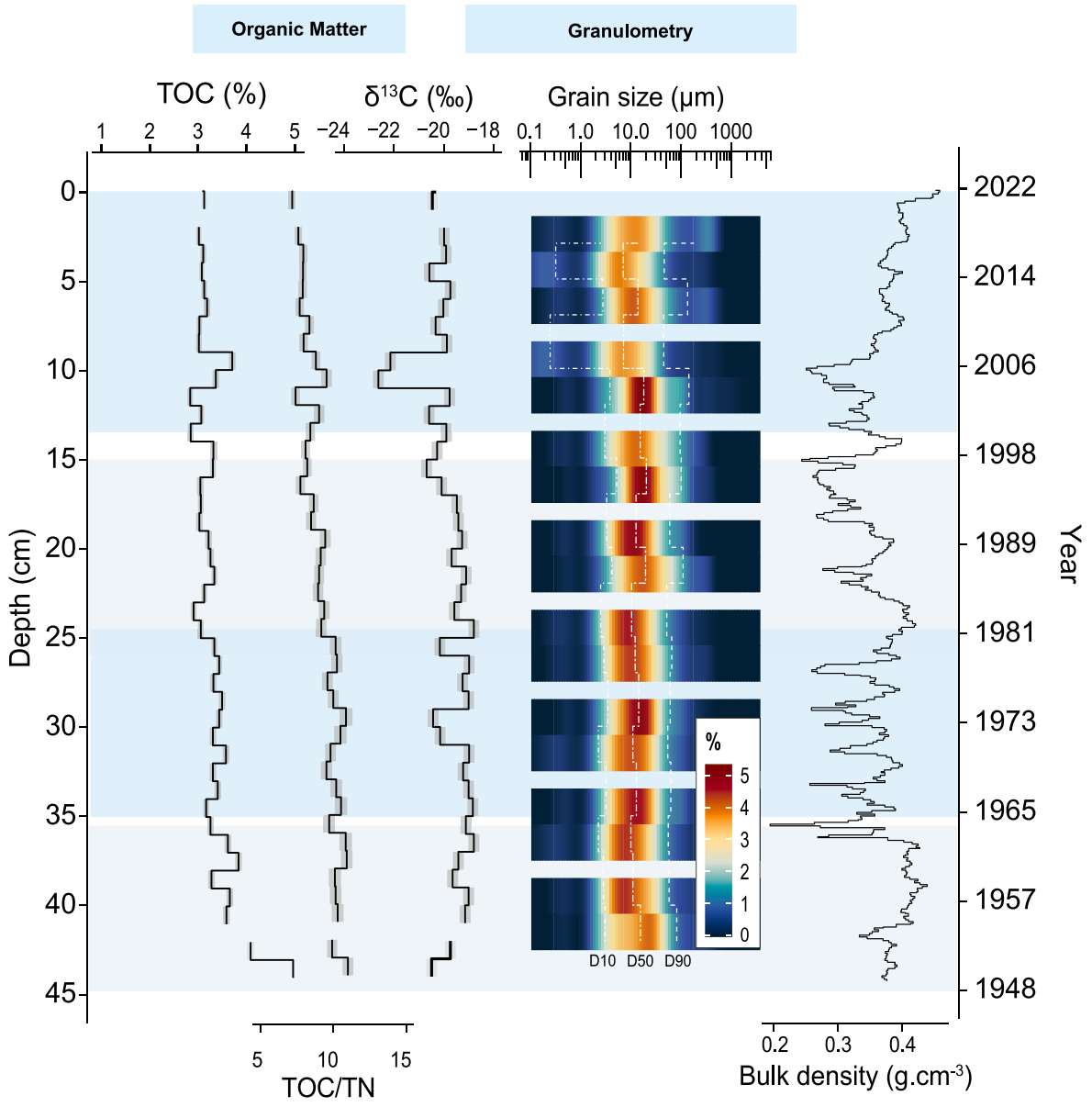

Fig. 3. Results of Rincón del Bonete core analyses, including organic matter properties (TOC in % and TOC/TN), grain size distribution with D10, D50 and D90 values (dashed white lines) and bulk density values.

while autochthonous matter is usually characterised by values below 10. Organic matter in the reservoir therefore appears to consist of a mix of allochtonous and autochthonous material.

A correlation of $r^2 = 0.7$ is obtained between the measured density and the CT-scan value (Fig. A.1). The density obtained from calibrating CT-scan values ranges between 0.19 and 0.58 ± 0.05.

3.3. Radionuclide analyses and age model

3.3.1. Gamma spectrometry

The $^{210}Pb_{ex}$ activity along the core decreases following a well-constrained linear trend ($r^2 = 0.96$) when plotted using a logarithmic scale (Fig. 4). ^{137}Cs activities vary from negligible levels (<0.6 Bq kg^{-1}) at the base of the sequence to 12 ± 0.6 Bq kg^{-1}. The highest activities of ^{137}Cs are detected between 30 and 35 cm depths, and they are attributed to the peak of the maximum ^{137}Cs bomb fallout generally dated to 1964–1965 in the Southern Hemisphere (Foucher et al., 2021).

3.3.2. Plutonium analysis

$^{240}Pu/^{239}Pu$ ratios are found to vary between 0.069 and 0.264 (±0.066) along the core. According to the values of this ratio and their variations with time, four periods are identified with first, at the bottom of the core, high ratio values ranging between 0.232 and 0.264 (1948–1956) followed by a decrease in this ratio down to 0.180 (1961–1966). A low ratio between 0.069 and 0.101 is then measured from 1968 to 1981. Finally, a slight increase in this ratio is observed again in the upper part of the core, with corresponding ratio values of 0.114 and 0.096 for the period occurring between 2012 and 2018.

3.3.3. Age model

Age modelling of sediment cores is often achieved using the $^{210}Pb_{ex}$ method, with this initial model validation typically relying on ^{137}Cs activities, a radionuclide released during nuclear bomb tests conducted between 1945 and 1963 by the United States of America (USA), the Former Soviet Union (FSU) and the United Kingdom (UK). Along with

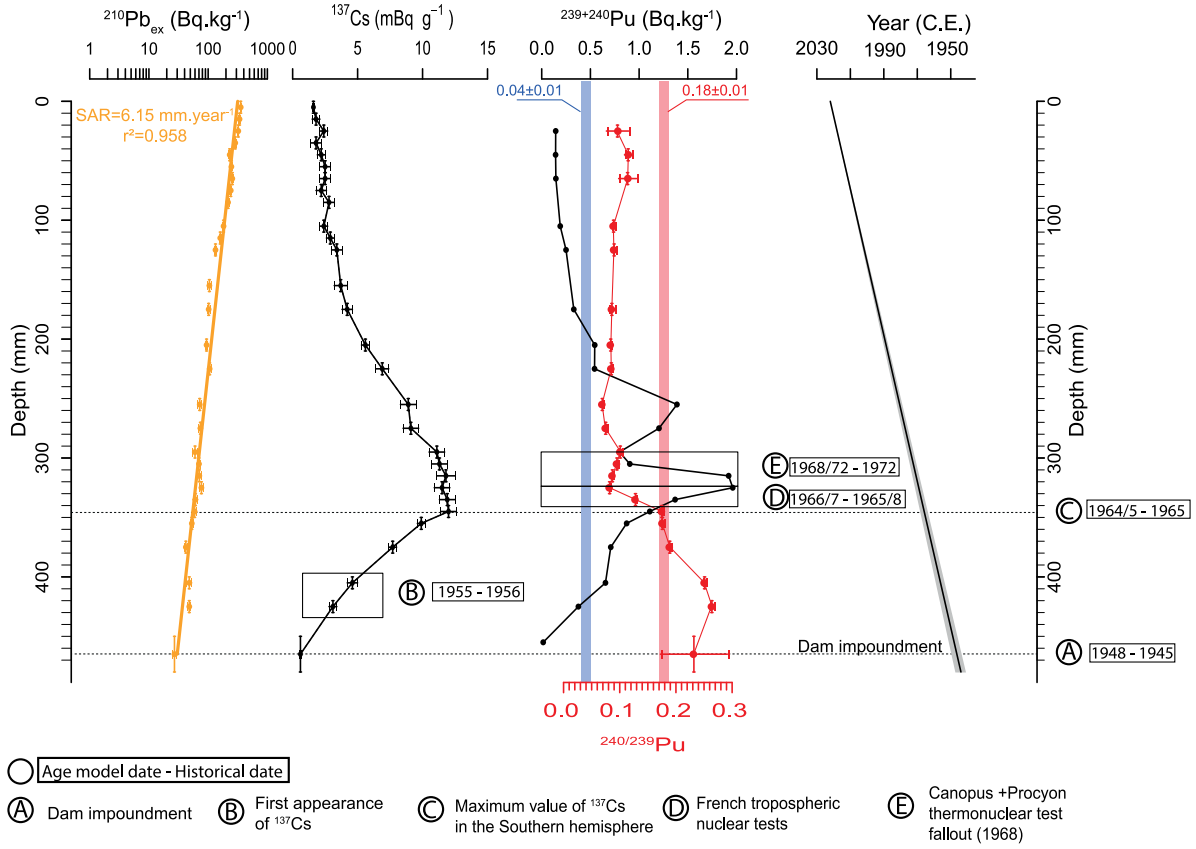

Fig. 4. Rincón del Bonete core profile with $^{210}Pb_{ex}$, ^{137}Cs, $^{239+240}$Pu activities (Bq kg^{-1}), $^{240/239}$Pu ratio and CFCS derived age model. Letters corresponding to historical events were added as well as the associated year.

Table 1
Comparison between the $^{210}Pb_{ex}$ age model and historical nuclear test events attributed on the basis of plutonium-related data as well as corresponding letters from figure 4.

Corresponding letter	Depth (cm)	Year attributed ($^{210}Pb_{ex}$ age model ±3 yr)	$^{240}Pu/^{239}Pu$ ($Bqkg^{-1}$)	Historical nuclear test events	Events
E	33 – 30	1968–1970	0.101 ± 0.002	1968–1972	Canopus/Procyon nuclear test fallout (launched 1968)
D	34 – 33	1965–1968	0.128 ± 0.001	1966–1967	French tropospheric nuclear test
C	35	1965	0.176 ± 0.003	1964–1965	Peak emissions of ^{137}Cs in the Southern hemisphere
B	42 – 40	1953–1956	0.251 ± 0.003	1955	First detection of ^{137}Cs

^{137}Cs, other radionuclides such as ^{239}Pu and ^{240}Pu were deposited globally during this period (UNSCEAR 2000 Report).

Age modelling or validation using ^{137}Cs in sediment cores collected in part of South America is controversial. Some studies have shown that the use of this radionuclide as an input for the validation of age models could be associated with significant uncertainties, given the wide shape of the peak observed in some sediment cores collected in this part of the world (Magand and Arnaud, 2007). Other radionuclides than ^{137}Cs may be used as stratigraphic markers (Ferreira et al., 2016). In this context, Chaboche et al. (2022) demonstrated that $^{240}Pu/^{239}Pu$ ratio could provide a powerful additional tool to validate the age model obtained with $^{210}Pb_{ex}$ and ^{137}Cs.

Application of the constant flux: constant sedimentation (CF:CS) model (Fig. 4) allowed dating the base of this 48-cm-long sequence to 1948 (±3 yr), which is in good agreement with the commissioning of the dam (1945), with an average sedimentation accumulation rate (SAR) of 6.15 ± 0.25 mm yr^{-1}. The first detection of ^{137}Cs in 1955 is dated to 1953 - 1956 (±3 yr, Table 1), which corresponds well to the common milestones used for dating in the literature (Foucher et al., 2021). The classical $^{210}Pb_{ex}$ approach allows for a good overall dating of the core, with the attribution of the bottom sediment layer to the creation of the dam reservoir in 1948. However, the ^{137}Cs maximum fallout attributed to 1964–1965 is not easy to identify in this core, as the peak between 30–35 cm is too wide to be attributed to sediment deposition during a single year. This maximum ^{137}Cs peak activity is dated with the $^{210}Pb_{ex}$ age model to 1965–1975. However, the $^{240/239}$Pu allows to refine the position of the ^{137}Cs peak emissions in the Southern hemisphere to 35 cm corresponding to 1965 with the CF:CS model and with a global fallout signature of $^{240/239}$Pu of 0.18 ± 0.01. In contrast, the rest of the peak is associated with the typical French nuclear test fallout signature (0.04 ± 0.01).

As a complement, variations in $^{240}Pu/^{239}Pu$ atom ratios and $^{239+240}$Pu activities provide insightful information about the differentiated timing of radioactive fallout sources of emission, therefore

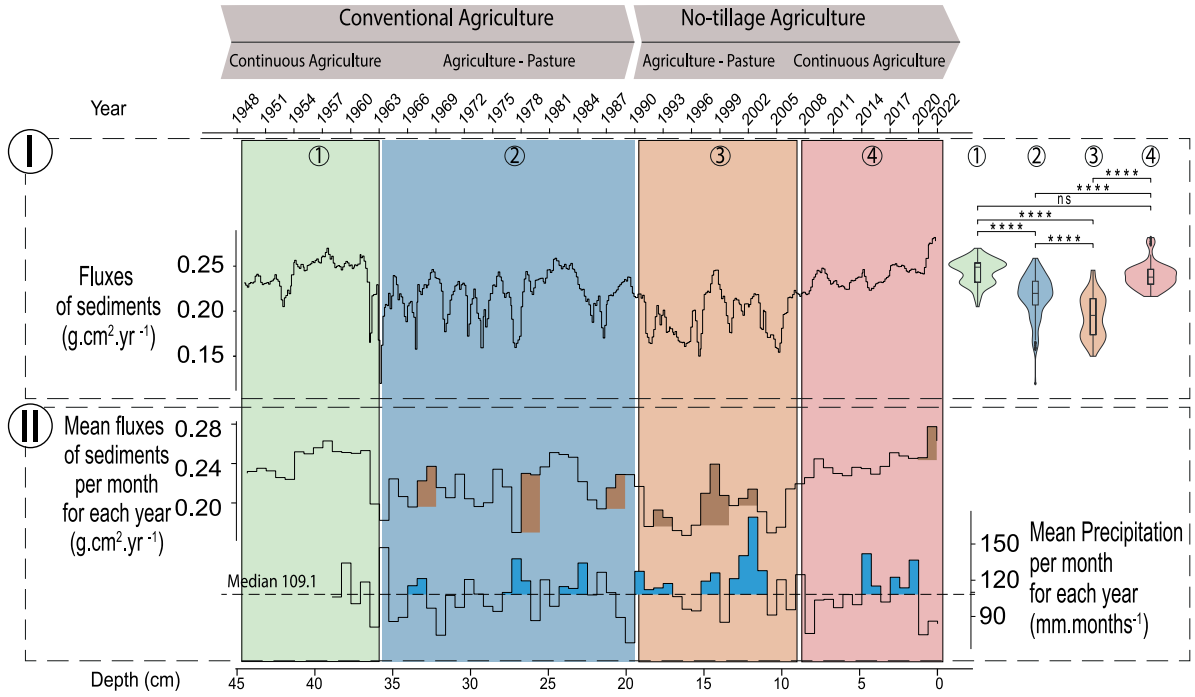

Fig. 5. Fluxes of sediments (MAR, I) and result of Dunn test on the MAR for the different periods of sediment delivery (I) and mean annual fluxes of sediment and precipitation (II). Periods of sediment delivery identified with the breakpoint test and their corresponding agricultural phases were added, in green, conventional continuous cultivation, in blue, conventional cultivation with rotation (agriculture-pasture). In orange, no-tillage cultivation with rotation (agriculture-pasture) and in red, no-tillage continuous cultivation.

allowing the overall validation of the age model. Indeed, depending on the type of bomb used and the usage period, as they changed with time, contrasted $^{240/239}$Pu atom ratios were obtained (Koide et al., 1985). USA, FSU and UK bomb testing contributed to a pre-moratorium global fallout signature of 0.18 (Chaboche et al., 2022), which corresponds to the mean $^{240/239}$Pu ratio of fallout that was emitted in the atmosphere from 1945 to 1963. French nuclear bomb testing in the Southern Hemisphere started later in 1966–1974 and was found to be detectable in South America (Chamizo et al., 2011). This can explain the wider peak of ^{137}Cs observed in the core, likely consisting of the mix of the bomb fallout peak commonly attributed to 1963 (or 1964–65) followed by the significantly lower $^{240/239}$Pu signatures (around 0.04) fallout levels associated with French bomb testing conducted in French Polynesia (1966–1974). During this later phase among which the French troposphere nuclear tests (1966–1967) are likely observed in the core from 34–33 cm, with a change from higher to lower $^{240/239}$Pu ratios (attributed to 1965–1968) and the first H bomb nuclear test fallout, Canopus and Procyon (1968–1972) observed in the core from 33–30 cm and attributed to 1968–1970. These events were identified based on findings published by Chaboche et al. (2022) and are summarised in Table 1.

3.4. Rainfall evolution

TerraClimate rainfall data in the Rincón del Bonete catchment during the 1958–2023 period shows large variations between 817 and 2067 mm.yr^{-1} (Fig. A.2).

The Mann–Kendall trend test reveals a positive trend in rainfall with a τ of 0.02, although with a p-value of 0.79 for the 1958–2023 period.

The mean precipitation per month for each year of the precipitation dataset as well as the final median for the mean precipitation was calculated. Periods of multiple years with higher precipitation than the median were identified in the precipitation dataset. The reconstructed rainfall shows periods of higher mean precipitation than the median for multiple years in 1967–1968, 1977–1978, 1981–1984, 1986–1987, 1990–1993, 1997–1998, 2000–2003, 2014–2015 and 2017–2019 (Fig. 5, II).

3.5. FLUXES OF SEDIMENTS

The MAR ranges between 0.12 and 0.28 ± 0.06 g cm^2 yr^{-1} (Fig. 5I). These values are similar to those found by Foucher et al. (2023), in which values ranged from 0.10 to 0.20 and from 0.13 to 0.19 g cm^{-2} yr^{-1} for the Rincón del Bonete and Palmar (reservoir located a bit further downstream on the Rio Negro river) sediment cores, respectively. However, higher maximum values are found in this study (maximum 0.28 ±g cm^{-2} year^{-1}).

The breakpoint tests applied to the MAR suggest the occurrence of the three breakpoints in 1962, 1990 and 2007 (Table 2).

Although the Shapiro test result was close to 1 (Table 3), the probability of observing the result under null hypothesis was too low ($p < 0.0001$), thus violating the normality assumption. Therefore, a Kruskal–Wallis test was chosen instead of the well-known ANOVA test to compare the different periods.

The Kruskal–Wallis test on the four different periods (conventional and no-tillage with and without pasture, Table 3) shows that a least one of the period significantly differs from the others and post hoc test were therefore conducted.

Post hoc analysis reveals significant differences between pairwise comparisons (Table 3).

Based on the historical records and the existing literature identified in Section 3.1, these four periods of sedimentation identified align well with the distinct phases in Uruguay's agricultural development. The four distinct periods of sedimentation identified are characterised first by a plateau with high MAR values is observed (average value of 0.24 ±0.01 g cm^{-2} yr^{-1}) between 1948 and 1962, followed by a period of strong variations between 1962 and 1990 (average value of 0.22 ±0.02 g cm^{-2} yr^{-1}, overall range: 0.11–0.26 g cm^2 yr^{-1}). The 1991–2002

Table 2
Results of statistical breakpoint test on MAR via the breakpoints package (Hurtado et al., 2020).

Test	Breakpoints date - p value		
Pettit	1962 - $3.2e^{-27}$	1991 - $8.6e^{-11}$	2008 - $4.0e^{-15}$
Buishand	1962 - 0	1991 - 0	2006 - 0
Historical dates	≈1970	≈1990	≈2002

Table 3
Results of statistical tests Shapiro–Wilk (W measures how closely data follows a normal distribution, the closer to 1 the more normally distributed are the data and p the probability of observing the result under the null hypothesis), Kruskal–Wallis (χ^2 from 0 to infinite, the closer to 0 the more similar are the medians of the groups tested, and p the probability of obtaining a test statistic equal to or more extreme than the observed χ^2) and Dunn (Statistic gives the difference between mean ranks of two groups from negative to positive infinite, p the *p*-value measured from statistic, p.adj the p adjusted from Bonferroni method and p.ajd.signif the significance annotation from non significative, ns, to highly significative, *****) on the MAR. C and NT stand for the conventional and no-tillage periods. -Ct and -PR stand for continuous cultivation or cultivation with pasture rotation respectively.

Shapiro–Wilk	Normality Test	W = 0.98	p < 0.0001	Data	violated	normality	
Kruskal–Wallis	Comparison	$\chi^2(3) = 218.26$	$p < 2.2e^{-16}$	Significant	differences	in groups	
Dunn							
Periods Compared		Number of observation		Statistic	p	p.adj	p.adj.signif
C-Ct	C-PR	81	181	−8.65	$4.91e^{-18}$	$2.95e^{-17}$	****
C-Ct	NT-PR	81	101	−12.86	$7.00e^{-38}$	$4.2e^{-37}$	****
C-Ct	NT-Ct	81	91	−1.74	$8.18e^{-02}$	4.91e−01	ns
C-PR	NT-PR	181	101	−6.13	$8.52e^{-10}$	$5.11e^{-09}$	****
C-PR	NT-Ct	181	91	6.93	$4.06e^{-12}$	$2.43e^{-11}$	****
NT-PR	NT-Ct	101	91	11.43	$2.70e^{-30}$	1.62e−29	****

period is then characterised by a decrease in sediment inputs (mean: 0.19, ±0.02 g cm^{-2} yr^{-1}), whereas the period between 1991 and 2022 shows a new acceleration (mean: 0.23, ±0.01 g cm^{-2} yr^{-1}). Notably, the recent years (2019–2022) display the highest values observed along the entire sediment core (mean: 0.26, ±0.01 g cm^{-2} yr^{-1}, max: 0.28 in 2021).

The transition dated to 1962 took place somewhat earlier compared to the expected history in Uruguay, where the transition to conventional agriculture with pasture rotation took place between 1970 and 1980. However, it can be hypothesised that sediment delivery was influenced by the processes that occurred in the Brazilian part of the river basin, which started its intensification already in the 1960s (Pereira et al., 2012).

The largest difference is observed between the MAR during the conventional period with continuous cultivation and the MAR during the no-tillage period with pasture rotation (p.adj < $2.45e^{-36}$), with no-tillage practices showing significantly lower sediment fluxes. Similarly, the no-tillage period with continuous cultivation has a significantly lower MAR compared to most other groups (p.adj < $5.13e^{-19}$).

A smaller but still significant difference is observed between the MAR during the conventional period with pasture rotation and the MAR during the no-tillage period with continuous cultivation with p.adj = 0.0079 (Table 3). This suggests that incorporating pasture into conventional systems contributed to reduce sediment flux, but not as much as the change to no-tillage practices.

Despite the lack of historical data for the Rincón del Bonete reservoir prior to 1985, the history of agriculture in Uruguay suggests that more land was likely cultivated or used for ranching during the first period compared to the second, with conditions similar to those of the third period (Hudson et al., 1992). High sediment fluxes were observed during this initial period of conventional tillage, followed by a reduction associated with the introduction of conservation measures in 1981 (Law No. 15239) (Zurbriggen et al., 2020), pasture–crop rotation and a reduction in cultivated areas.

The transition to no-tillage practices and afforestation in the early 1990s further reduced sediment fluxes, although as cultivated areas increased. Continued use of pasture–crop rotation and afforestation contributed to temporary reductions in sediment delivery, despite the ongoing expansion of agriculture.

However, from 2007 onward, sediment fluxes increased again, coinciding with a shift toward continuous and double cultivation systems, intensification of land use, and increased wood harvesting. Land-use and land-cover changes during this period were driven not only by national agricultural policy but also by global trade dynamics. Nearly 80% of land-use land-cover changes since 1995 are linked to rising exports from Latin America, Africa, and Southeast Asia (Cabernard et al., 2024). This period also saw a significant expansion of genetically modified soybean cultivation (Foucher et al., 2023). These findings confirm the acceleration of sedimentation rates identified in recent years by Foucher et al. (2023), and highlight the impact of agricultural intensification on erosion.

Based on the $\delta^{13}C$, some events were identified. During the second peak of $\delta^{13}C$ (2004–2005), the observed values exhibit a tendency to reach lower levels than the first peak (i.e.−22.6‰). This phenomenon could be indicative of the incorporation of more C_3 photosynthetic pathway plants from the river basin, corresponding to the implementation of soybean and eucalyptus or the removal of previous paddy fields cultivated with rice.

Some rice was still cultivated in the river basin in 2020/2021 (Ministerio de Ganadería, Agricultura y Pesca) and used to be widely cultivated in the river basin in the past. Therefore, this second peak of $\delta^{13}C$, could correspond to the removal of previous paddy fields cultivated with rice.

Conversely, this second peak of $\delta^{13}C$ coincides with that of temporary crops observed in the river basin in 2004–2006 (with a 21% increase from 2003 to 2004–2006), which tends to rather confirm the first hypothesis of the massive introduction of soybean in the river basin.

This soybean expansion, which took place in the aftermath of the 2002–2004 economic crisis in Uruguay, could be explained by the high taxation of agriculture in neighbouring Argentina, as this policy included elevated soybean export taxes (Zurbriggen et al., 2020). In the absence of such taxation in Uruguay, it granted a favourable financial climate for soybean cultivation in this country.

Furthermore, exotic trees and mainly eucalyptus, another C_3 plant, were known to have been harvested during the same period (Foucher et al., 2023). Therefore, in a context of a mix of C_3-C_4 plants, the peak of $\delta^{13}C$ that we observe could correspond to the massive introduction of C_3 plants, either corresponding to the expansion of the soybean area or the planting of eucalyptus trees in the river basin, or to both.

In addition to the land-use and land-cover, the potential impact of the precipitation factor on the sediment dynamics was also investigated.

Since the fluxes of sediments and precipitation were not sampled with the same frequency, comparison was complex, therefore the mean annual fluxes of sediments per months were calculated, and when compared with the mean precipitation per month for each year, different temporal patterns are found for distinct periods (Fig. 5II). Precipitation were found only from 1958 and no period of multiple years with higher precipitation than the median (wet period) was considered between 1958–1964. The second period (1964–1990) shows some correlation between both variables. The different wet periods investigated likely generated events associated with higher sediment delivery, while drier periods were likely correlated with periods of lower sediment delivery. Supplementary analyses were conducted to quantify the impact of precipitation on sediment fluxes. However, the irregular rate frequency of sediment fluxes did not allow for quantification of the impact of each individual rainfall event identified in the precipitation sequence.

During the third phase (1990–2007), two wet periods are found in the precipitation, which probably impacted the sediment fluxes. However, it can be seen that the wet intervals only has a limited influence, if any, on the fluxes of sediment during this second phase.

In contrast, the fourth and final phase (2007–2023) is characterised by a clear decoupling between sediment fluxes and precipitation variability. Indeed, the wet period observed in 2017–2019 had a disproportionate effect on the fluxes of sediments with a much higher sediment peak observed for rainfall episodes although they remained of the same order of magnitude as those recorded during the previous phase.

The precipitation dataset was selected to cover the longest period possible. However, its monthly resolution limited the ability to analyse short-term, high-intensity erosion-prone rainfall events, which may represent a significant source of variability in sediment fluxes. Future studies could benefit from incorporating higher-resolution daily precipitation datasets available for more recent periods, enabling a more detailed assessment of the relationship between extreme rainfall and sediment dynamics.

3.6. Pesticides

Of the 16 pesticides analysed, 13 substances were detected in the core with various concentrations and fluxes (mol cm^{-2} yr^{-1}, Fig. 6). Post-depositional mobility may be an issue for all pesticides. Therefore, the first detection depth and production date of each compound as well as the comparison with historical events, such as field trials and usage recommendations in Uruguay (Nuevos herbicidas para cultivos de invierno) were used to select those substances with minimal mobility along the profile. Glyphosate and its metabolite AMPA are excluded from this discussion due to excessive diffusion, as shown in the supplementary material (Fig. A.3). Mirex is not detected in the core. All the pesticides data treated in this section (3.6) are shown in Fig. 6.

3.6.1. Herbicides

With the exception of Diuron, which is detected from 1955 onwards, all herbicides (in the green portion in Fig. 6) are found from the 1975–1985 period. The fluxes of Diuron (marketed from 1954 Woodford, 1957), similar to those of Simazine and Atrazine (marketed from 1956 and 1958, respectively Heri et al., 2008), decline from the 1980/1990s before reappearing from 2010 to 2022. After the first widespread use of herbicides observed in the 1970s, their usage decrease and they are only significantly used again from 2005 onwards. After its first introduction, S-Metolachlor, marketed from 1976 (United States Environmental Protection Agency - Reregistration Eligibility Decision (RED) Metolachlor), is found in low levels until 2018 when high fluxes are detected again. Diuron is used to control undesirable grasses and other annual and evergreen broadleaf weeds. This herbicide usage was first reported in Uruguay in 1967 (Merotto et al., 2022). Therefore, the first peak of Diuron in 1955 to 1960 probably corresponds to diffusion. However, the second peak from 1967 corresponds with the first reported use of this herbicide in Uruguay. It is detected in the core during a period devoid of afforestation. Therefore, this herbicide detection might be attributed to the initial disturbance of the Pampa, mainly in the Northern part of the river basin in order to remove annual grasses. In the 1970s, Diuron was also recommended in Uruguay to be used for cultivating winter wheat (Nuevos herbicidas para cultivos de invierno). Nevertheless, no cultivation of wheat was documented in the river basin. Otherwise, some rice was still cultivated in the river basin in 2020/2021 (Ministerio de Ganadería, Agricultura y Pesca) and used to be cultivated in the river basin in the past. Therefore, Diuron might also have been used as a pre-emergence herbicide in paddy fields in order to control annual weeds. This could also explain the detection of the first peak of $\delta^{13}C$ observed in 1973 (around 30 cm; Fig. 3) corresponding to the degradation of paddy fields through the use of Diuron and the supply of C_3 plant residues to the reservoir.

2,4-D, which was first tested in the 1940s (Merotto et al., 2022) in Uruguay, is detected in the core from 1950 onwards. This herbicide was likely used to destroy the weeds under the crops. It is detected in greater quantities simultaneously with the appearance of S-Metolachlor, Simazine and Atrazine, which are detected in the sediment core from 1975, periods during which all the herbicides started to be generally used in Uruguay. These herbicides were likely used for pre- and post-emergent treatments of annual weeds (Merotto et al., 2022). The rise in multiple herbicides in the 1970s could be related to the cereal and oilseed boom period that took place in Uruguay at that time for land preparation and weed control (Merotto et al., 2022). Furthermore, the rise of Atrazine from 2007 could be linked with the increase in temporary crops and the preparation of the grasslands to plant soybean.

Diuron is the first herbicide to be detected in the core in significant quantity and its concentration decrease from the 1970, which corresponds to the rise in multiple other herbicides (S-Metolachlor, Simazine, Atrazine and 2,4D). Therefore, it can be hypothesised that Diuron was replaced from the 1970 with the other herbicides detected afterwards.

3.6.2. Fungicides

The Tebuconazole fungicide (in the red portion in Fig. 6) starts to be detected significantly in the core from the late 1980s onwards, with increasingly higher fluxes until 2018. This fungicide has been mainly used in large scale crop-fields to prevent different types of plant diseases (Tleuova et al., 2020) and could be representative of the implantation of soybean cultivation for which this fungicide has been recommended for. Furthermore, this detection is in good agreement with the massive expansion of soybeans that took place from 1990 in the river basin, as shown by Foucher et al. (2023).

3.6.3. Insecticides

The insecticide DDT was freely marketed from 1945 (Mellanby, 1992) to 1968 when it was banned in Uruguay (Mañay et al., 2004). This insecticide and its metabolites, DDE and DDD, are detected from 1948 (±3) in the core (in the grey part in Fig. 6). Three peaks of DDT are measured, the first from 1948 to 1970, the second in the 1990's and, finally, the third from 2005. DDD and DDE fluxes increase until 1985 when they dropped, before increasing again from 2005 and 2010 respectively. They remain high along the sediment profile, except for a drop observed before the 2000s and an increase afterwards. DDT is

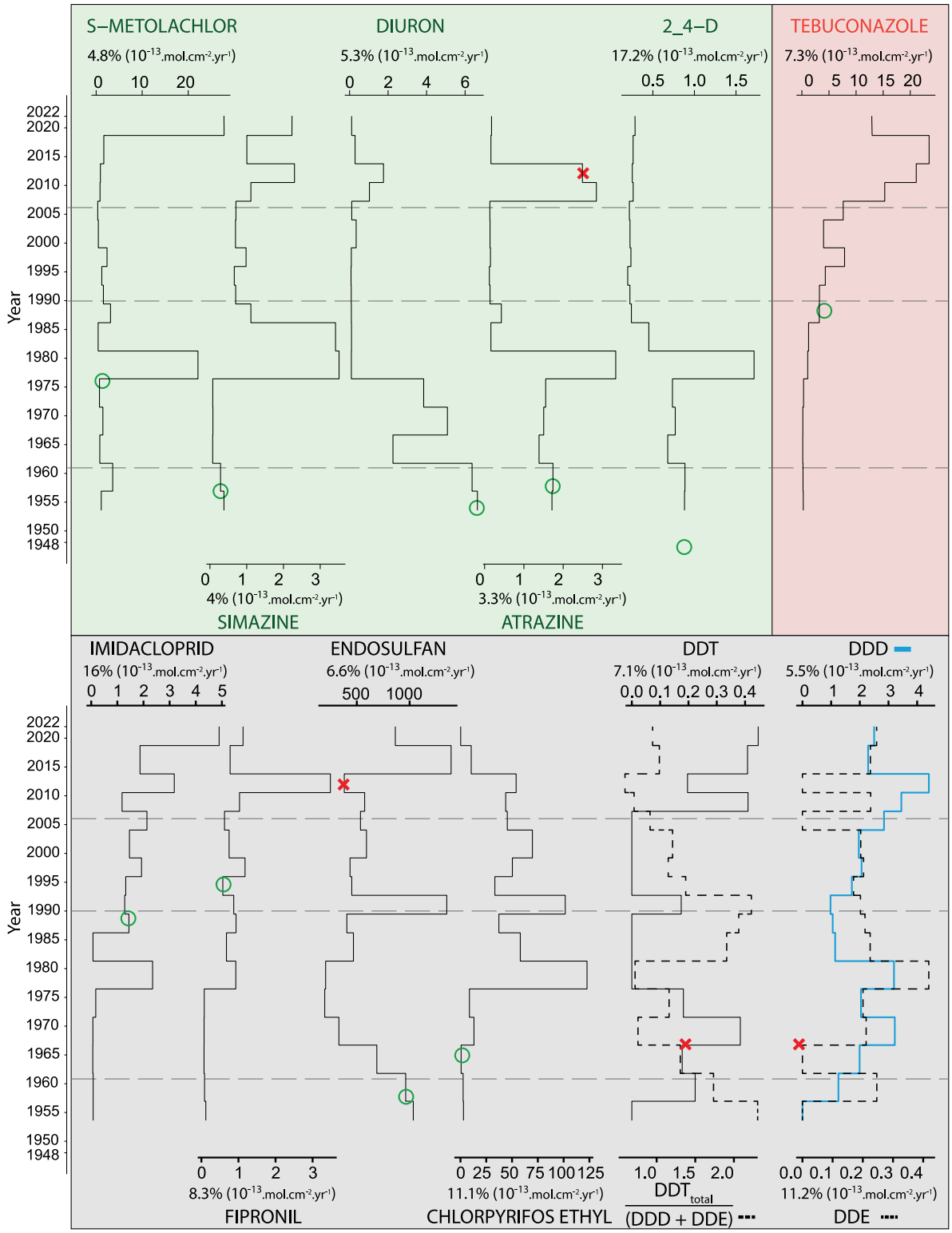

Fig. 6. Fluxes (in 10^{-13} mol cm^{-2} yr^{-1}) of insecticides (grey), herbicides (green), and fungicides (red). Uncertainty for each pesticide is indicated alongside its range. The date of production is marked with a green circle, and the date of ban with a red cross.

considered to diffuse at a rate of 10^{-8} cm^2 s^{-1} (Logan et al., 1989), but this movement generally takes place downward and not upward. The peaks of DDT and its metabolites observed therefore correspond to events that occurred in the river basin and not to post depositional mobility.

Several hypotheses may be put forward for explaining the source of DDT and its metabolites along the profile. To test these hypotheses, DDD and DDE, respectively the anaerobic and aerobic metabolites of DDT, produced depending on the degradation conditions of the pesticide (PubChem - DDT) can provide better insights into the origin of the second and thirds peaks observed in the 1990s and after 2007.

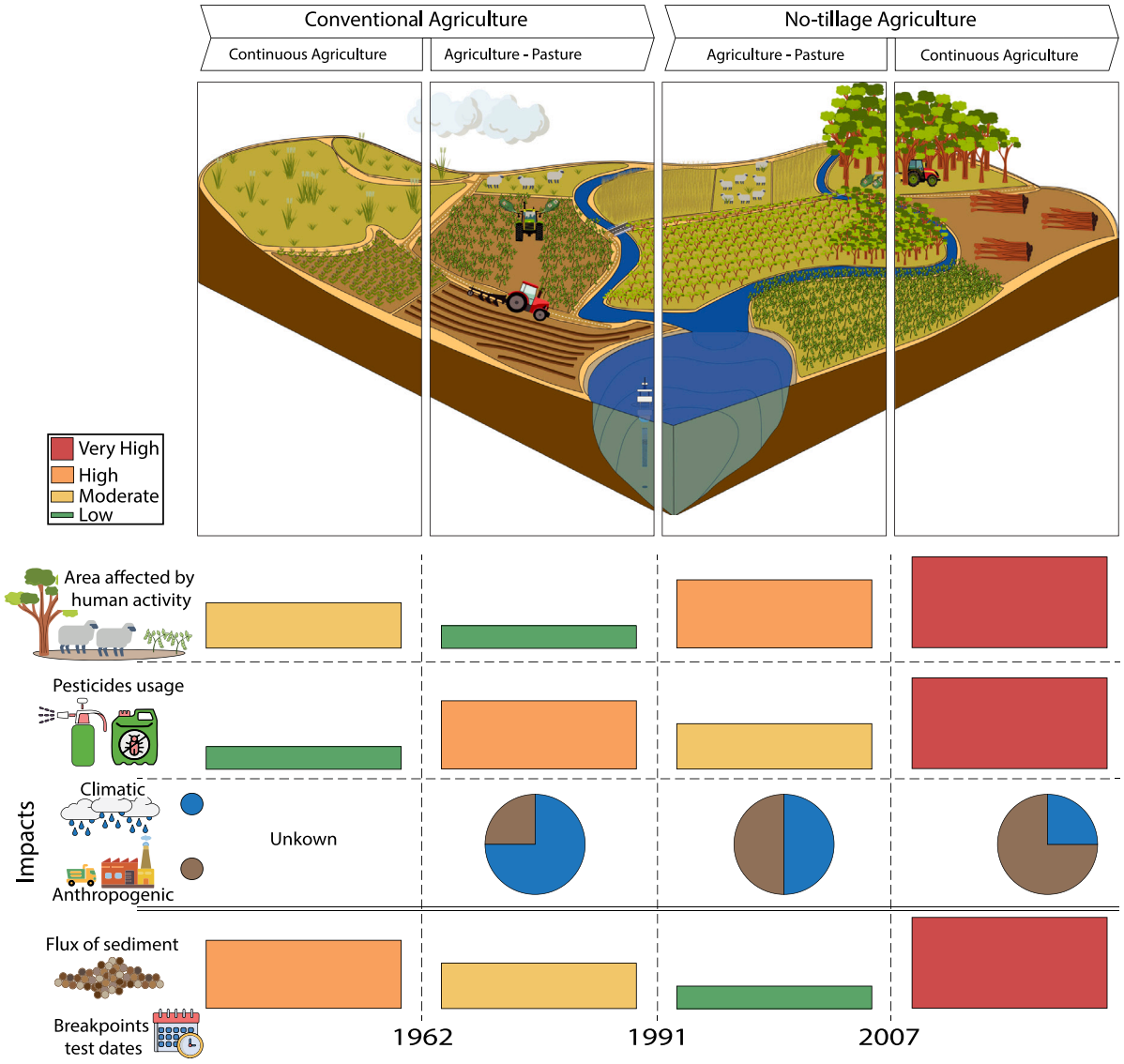

Fig. 7. Synthesis of the main findings of this study and conceptual representation. The **Area affected by human activity** was derived from land-use land-cover analysis, **pesticide usage** from the pesticide analyses, **climatic and anthropogenic impacts** from the sediment flux/precipitation comparison, and the **sediment flux** and **breakpoint test dates** from MAR analysis. Results were categorised by period and expressed on a scale ranging from low to very high.

First, the DDT may have been supplied during the same period of original application before the 1970s when attempts to eradicate yellow fever, malaria and other vector-borne diseases were put in place. In fact as reported in Severo (1955), the plan to eradicate both *Anopheles* and *Aedes aegypti* mosquitoes, the primary vectors of malaria and yellow fever, respectively, initiated in Brazil as early as in 1932, was generalised to the whole continent at the end of World War II. From 1948 to the early 1970s, DDT was used extensively in and around potential habitats of the insect in an attempt to eradicate it. Therefore, the reappearance of DDT from 2007 could be due to the erosion of previously undisturbed soils that had been contaminated with DDT, corroborating the rise in herbicide use, such as Atrazine, since 2007.

This study suggests that the secondary peak of DDT observed in the sediment core may be due to a newly applied insecticide, rather than the remobilisation of a previously applied substance.

In fact, Dicofol, an organochlorine insecticide (PubChem - Dicofol), marketed since 1955 and structurally similar to DDT world health organisation - food and agriculture organisation of the united nations, which was not analysed in this study, was detected as a source of DDT contamination in previous studies (Turgut et al., 2009). As Dicofol can be synthesised using DDT, large amounts of DDT impurities may be found in Dicofol. Turgut et al. (2009) found between 0.3 to 14.3% of DDT in the Dicofol that they analysed. Barra et al. (2006) reported the use of Dicofol in South America. For example, in 2000, Brazil imported 111 tonnes of Dicofol and produced 209 tonnes of this substance. Furthermore, according to Travis et al. (2020), one commercial formulation of Dicofol was approved for use in the country and they also showed the presence of Dicofol residues on children wrists in Uruguay. Despite the fact that no specific link could yet be made between Dicofol and DDT exposure in Uruguay (Travis et al., 2020), the impurities found in Dicofol and its potential use in Uruguay could be the cause of the second peak of DDT and its metabolites observed in the core in the 1990's.

However, more investigation is required to verify the hypothesis of an indirect DDT contamination due to the use of Dicofol in the river basin.

Endosulfan is also detected in 1948 and the associated fluxes decrease until 1980. Two peaks are then observed in 1990–2000 and, more recently, from 2010 onwards, with a maximum recorded after 2015. Endosulfan was used for general pest control. In the 1990s,

organochlorine insecticides were banned in Uruguay (Boroukhovitch, 1998). Endosulfan was an exception (Boroukhovitch, 1998) and may therefore have provided an alternative to all these banned insecticides. The second peak observed in the core after 2010 probably corresponds to the use of the remaining stocks of Endosulfan after it was banned in 2011 (Registro Nacional de Leyes y Decretos).

Chlorpyrifos Ethyl, first registered in 1965 in the United States of America (Rauh et al., 2011), is found in the core in high proportions from 1975. This broad-spectrum insecticide is widely used on various crops, in public health programs, particularly for the control mosquito, ants, cockroaches, and certain disease-carrying tick species. In the sediment core, the rise of Chlorpyrifos-Ethyl coincided with the decline of DDT, suggesting it may have been adopted as a replacement substance following the ban on DDT.

Finally, Imidacloprid and Friponil are first detected in 1975 and the associated fluxes continued to increase until nowadays. Friponil peaks between 2010 and 2018 whereas Imidacloprid increases from 2000 to 2022. Imidaclopride was the first neonicotinoid discovered in 1985 and Friponil, a phenylpyrazole, was discovered in the 1990. These insecticides were developed in response to increasing pesticide resistance to other compounds (Jeschke et al., 2019). Both insecticides are used as seed coating and could have been introduced in the river basin during the increase of temporary crops observed from 1985. However, some diffusion associated with these substances can be observed in the profile and care was therefore taken when interpreting the temporal evolution of the fluxes of these insecticides.

4. Conclusions

Key findings of the study have been summarised and illustrated in Fig. 7. Each result has been categorised by period and expressed on a scale ranging from low to very high.

Through a comprehensive and original multi-proxy approach, this study revealed how changes from natural to human-dominated landscapes with massive introduction of monocultures and shifts in agricultural practices, have significantly affected sediment transport in the Uruguayan river basin, reflecting the trends observed across the Pampa biome.

- **Sediment fluxes** were found to **evolve concomitantly** with the **pesticide consumption** as well as the **land-use and land-cover change**, influenced in part by the **precipitation factor** in the early stages, and then dominantly controlled by the **anthropogenic actions** later on.
- The shift to **no-tillage** and **pasture rotation** briefly **reduced sediment fluxes**, despite the large amounts of herbicides required for this practice. However, the **intensification of agriculture** and **wood harvesting** later **reversed this trend**.
- Notably, two periods of **resurgence** of the banned **DDT** pesticide were observed in **recent years** (in 1990–1995 and from 2007). The present study suggests a possible **contamination** from a DDT-derived pesticide known as **Dicofol** followed by the **remobilisation** of previously applied DDT possibly resulting from the widespread use of this insecticide in attempts to eradicate the vector-borne malaria and yellow fever diseases after World War II.
- The **increase** in **sediment delivery** over the most recent period (**2008–2023**) is likely due to the **conversion of 12% of grassland over 14 years**, while 60% remain either natural or used for extensive ranching. As previously highlighted, large-scale land-use changes across South America are driven by the growing global demand for agricultural commodities. A striking example is the new UPM (UPM Uruguay) wood processing facility that has been built near the Rincón del Bonete dam, inaugurated in 2023 as the largest in Uruguay and one of the world's biggest factories of this type. With additional plants under construction, Uruguay's production capacity will continue to expand, emphasising the fact that the environmental degradation observed in the river basin reflects wider international market forces and requires global attention.

In future research, the contrasting landscapes (i.e. geology, soil types) and land-use of the Rincón del Bonete basin's two main tributaries deserve further investigation. Sampling at the outlet of each river and/or applying sediment fingerprinting techniques could help differentiate sediment sources and their potential variations with time, offering a more accurate understanding of erosion dynamics and land-use impacts within this river basin, representative of the situation observed across the wider Pampa biome.

CRediT authorship contribution statement

Amaury Bardelle: Writing – original draft, Investigation, Formal analysis, Data curation, Conceptualization. **Renaldo Gastineau:** Writing – review & editing, Investigation, Formal analysis, Data curation. **Floriane Guillevic:** Writing – review & editing, Investigation, Formal analysis. **Anthony Foucher:** Writing – review & editing, Validation, Supervision, Conceptualization. **Pierre-Alexis Chaboche:** Writing – review & editing, Investigation. **José Antonio Corcho-Alvarado:** Investigation, Formal analysis. **Stefan Röllin:** Investigation, Formal analysis. **Guillermo Chalar:** Writing – review & editing, Resources. **Pierre Sabatier:** Writing – review & editing. **Marcos Tassano:** Writing – review & editing, Resources. **Nathalie Cottin:** Methodology. **Rosalie Vandromme:** Writing – review & editing, Supervision. **Olivier Cerdan:** Writing – review & editing, Supervision. **Christine Alewell:** Writing – review & editing, Funding acquisition. **Olivier Evrard:** Writing – review & editing, Supervision, Funding acquisition.

Declaration of Generative AI and AI-assisted technologies in the writing process

During the preparation of this work, the authors used ChatGPT and Deepl in order to improve the language of the script. After using this tool/service, the authors reviewed and edited the content as needed and take full responsibility for the content of the published article.

Declaration of competing interest

The authors declare that they have no known competing financial interests or personal relationships that could have appeared to influence the work reported in this paper.

Acknowledgements

Funding

The current research took place in the framework of the AVATAR project funded by the French National Research Agency (ANR-22-CE93-0001), which supported the PhD thesis of Amaury Bardelle. Collaboration between France and Uruguay for sediment sampling has been supported by an applied research project from the Fondo Maria Viñas funded by the National Agency of Research and Innovation (ANII, Uruguay), the CELESTE Lab International Research Project (IRP) funded by CNRS (French National Research Centre) and the CELESTE ClimatAmSud project (23-MATH-01). We are grateful to the DOSEO platform (Université Paris-Saclay, CEA, List) and especially to A.-C. Simon and M. Agelou for performing the tomography scanner measurements on the sediment core.

Appendix

See Figs. A.1–A.3 and Tables A.1 and A.2

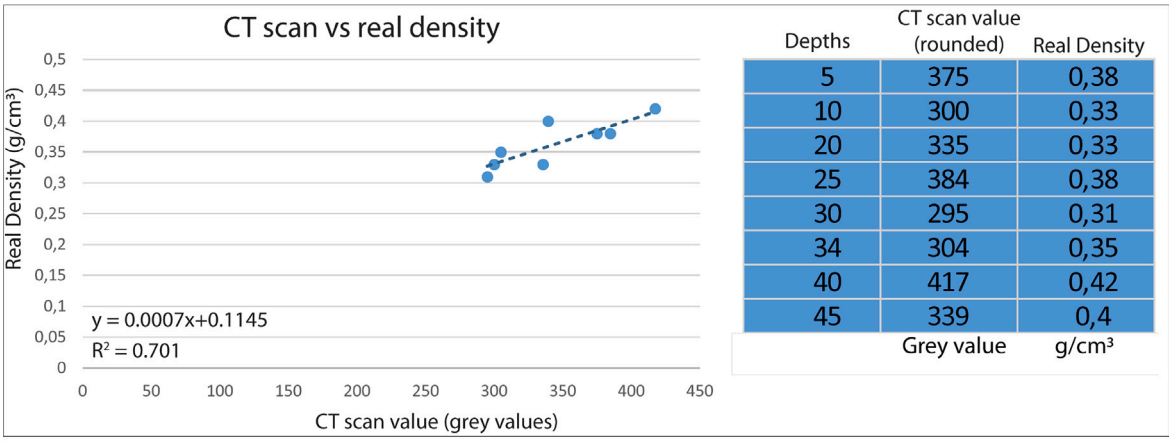

Depths	CT scan value (rounded)	Real Density
5	375	0,38
10	300	0,33
20	335	0,33
25	384	0,38
30	295	0,31
34	304	0,35
40	417	0,42
45	339	0,4
	Grey value	g/cm³

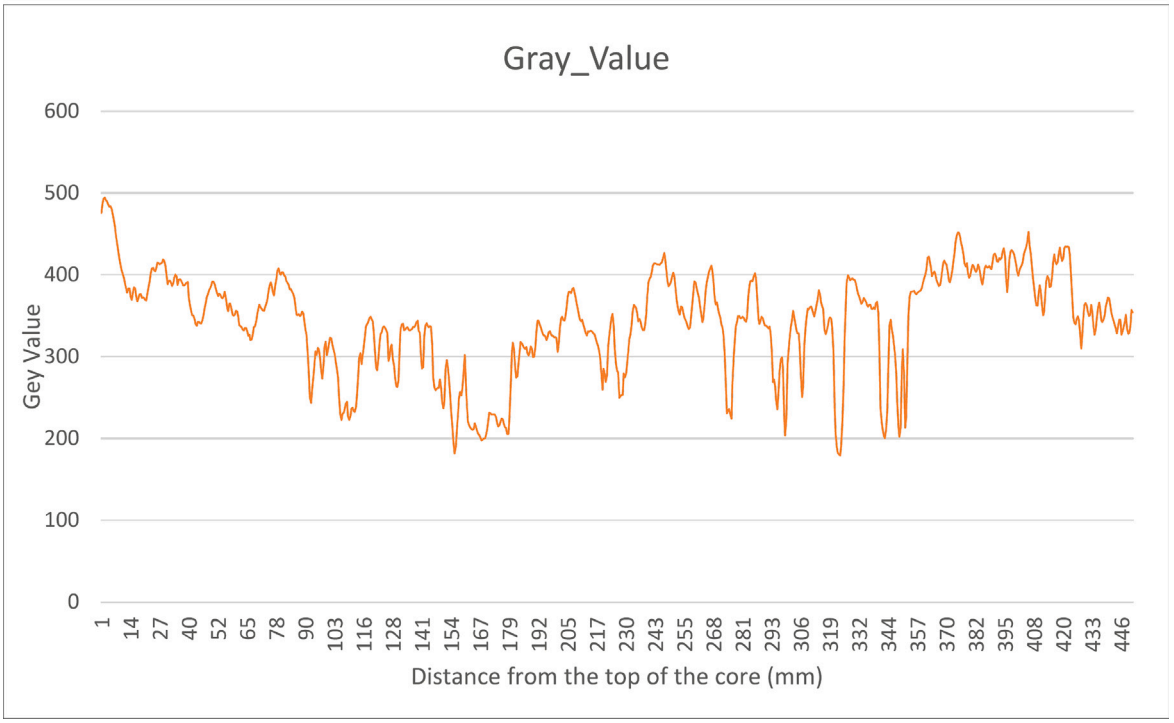

Fig. A.1. Correlation between measured density and CT scan values in blue in the top and CT scan values obtained in orange on the bottom part.

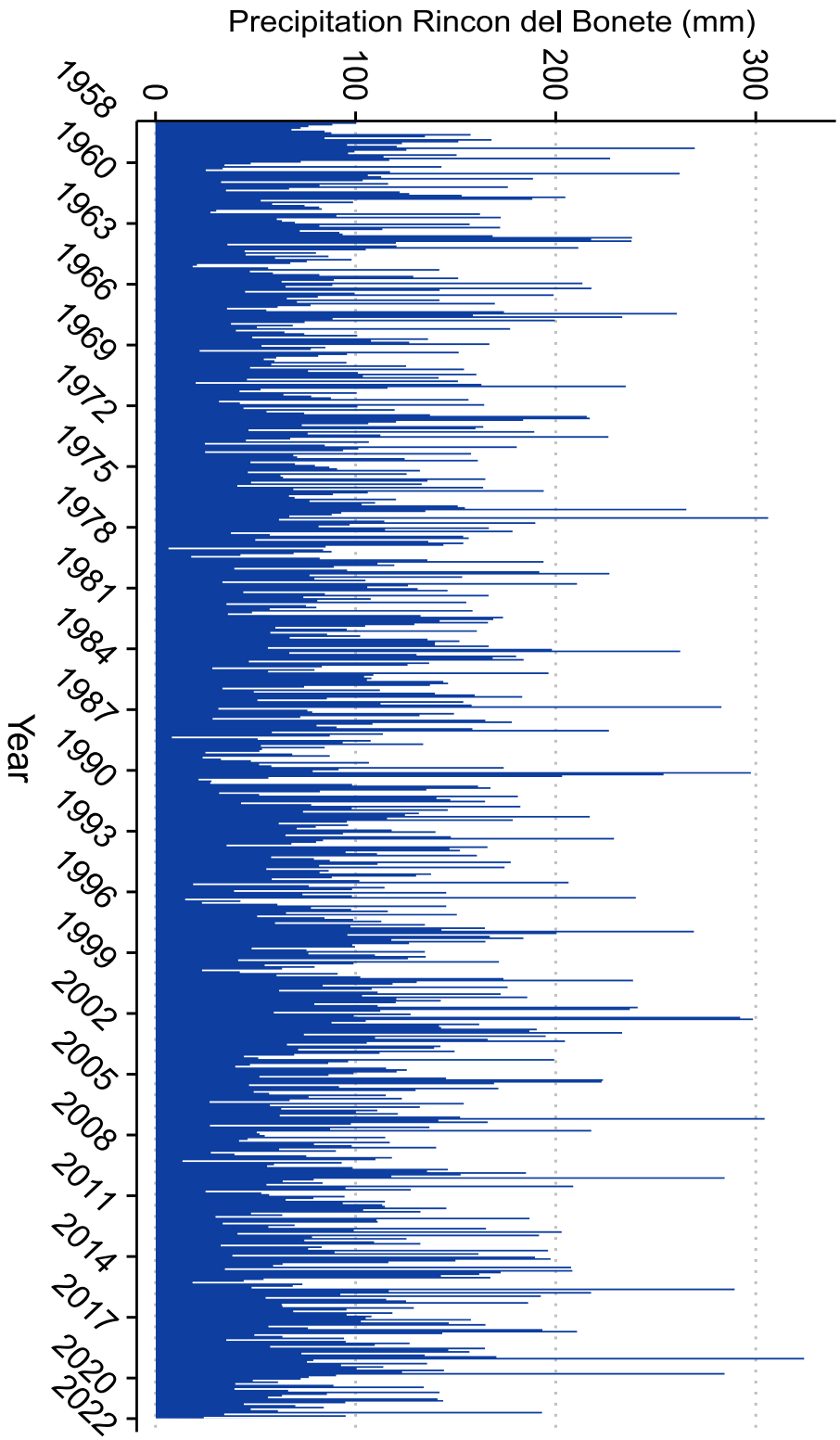

Fig. A.2. Monthly precipitation in the Rincon del Bonete river basin as recorded in the TerraClimate dataset.

Table A.1
Complete list of 16 pesticides with their abbreviations, International Union of Pure and Applied Chemistry (IUAPC) names and classifications. Molecules were found on PubChem (https://pubchem.ncbi.nlm.nih.gov/).

Pesticide	Abbreviation	IUPAC name	Family
2,4-Dichlorophenoxyacetic acid	2,4-D	2,4-Dichlorophenoxyacetic acid	Organic compound
Atrazine	Atrazine	6-chloro-N^2-ethyl-N^4-(propan-2-yl)-1,3,5-triazine-2,4-diamine	Triazine
Simazine	Simazine	6-chloro-N^2, N^4-diethyl-1,3,5-triazine-2,4-diamine	Triazine
Diuron	DCMU	3-(3,4-dichlorophenyl)-1,1-dimethylurea	Phenylurea
S-Metolachlor	S-Metolachlor	(S)-2-chloro-N-(2-ethyl-6-methylphenyl)-N-[(2S)-1-methoxypropan-2-yl]acetamide	Urea
Tebuconazole	Tebuconazole	(RS)-1-(4-chlorophenyl)-4,4-dimethyl-3-(1H-1,2,4-triazol-1-ylmethyl)pentan-3-ol	Neonicotinoid
Imidacloprid	IMI	1-[(6-chloro-3-pyridinyl)methyl]-N-nitroimidazolidin-2-ylideneamine	Neonicotinoid
Endosulfan	Endosulfan	dodecachlorooctahydromethanetriyl benzodioxathiepine oxide	Organochlorine
Fipronil	Fipronil	5-Amino-1-[2,6-dichloro-4-(trifluoromethyl)phenyl]-4-(trifluoromethylsulfinyl)-1H-pyrazole-3-carbonitrile	Phenylpyrazole
Chlorpyrifos Ethyl	Chlorpyrifos Ethyl	O,O-Diethyl O-(3,5,6-trichloropyridin-2-yl) phosphorothioate	Organochlorine
Dichlorodiphényltrichloroéthane	DDT	1,1'-(2,2,2-Trichloroethane-1,1-diyl)bis(4-chlorobenzene)	Organochlorine
Dichlorodiphényldichloroéthane	DDD	1,1'-(2,2-Dichloroethane-1,1-diyl)bis(4-chlorobenzene)	Metabolite of DDT
Dichlorodiphényldichloroéthylène	DDE	1,1'-(2,2-Dichloroethene-1,1-diyl)bis(4-chlorobenzene)	Metabolite of DDT
Glyphosate	Glyphosate	N-(phosphonomethyl)glycine	Phosphonate
AMPA	AMPA	(Aminomethyl)phosphonic acid	Metabolite of glyphosate
Mirex	Mirex	dodecachloropentacyclo[5.3.0.0^{2,6}.0^{3,9}.0^{4,8}]decane	Organochlorine

Table A.2
Summary of analysis conducted, parameters studied, resolution of the data, and units.

Analysis conducted	Studied parameters	Resolution	Units
Particle size analysis	D10, D50, D90	1 cm	μm
CT-scanner	Relative density	0.625 mm	Grey value
Bulk density	Bulk density	1 cm	g cm^{-3}
Organic matter analysis	TOC, TN, δ^{13}Corg	1 cm	% + ‰
Gamma spectrometry analysis	$^{210}Pb_{ex}$, ^{137}Cs	1 cm	Bq kg^{-1}
Plutonium analysis	^{239}Pu, ^{240}Pu	1 cm	Bq kg^{-1}
Pesticide analysis	See Table A.1 for full list	2–4 cm	mol cm^{-2} yr^{-1}
Fluxes of sediments	MAR	0.625 mm	g cm^{-2} yr^{-1}

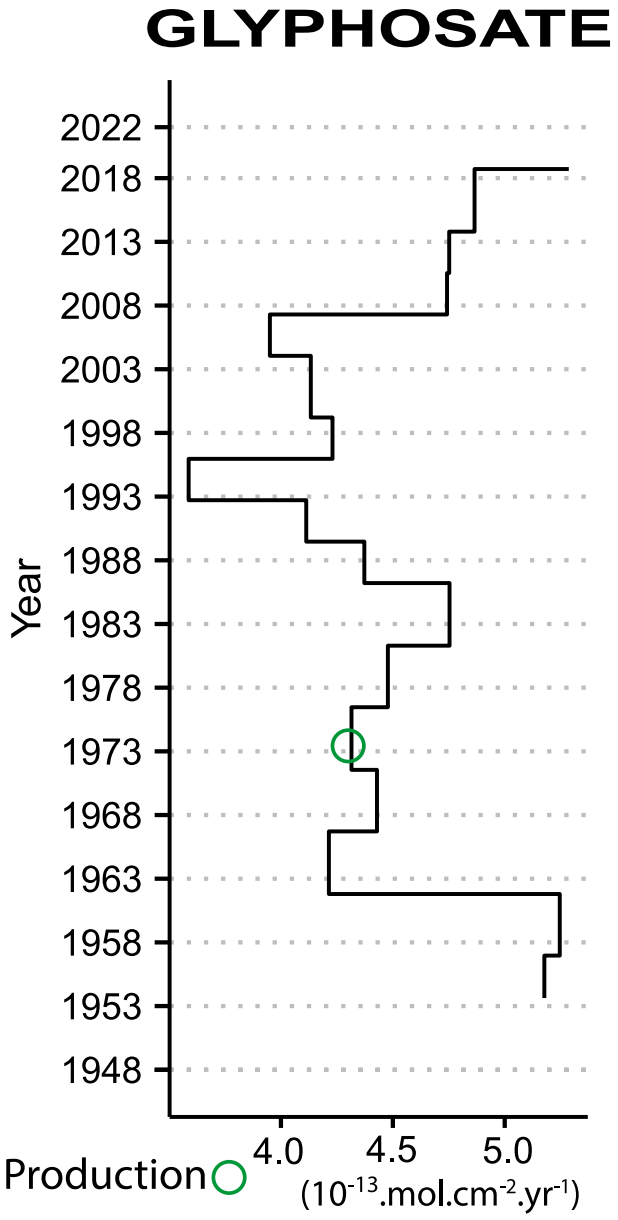

Fig. A.3. Fluxes of Glyphosate in 10^{-13} mol.cm^{-2} yr^{-1} ± 23.1%.

Data availability

I have shared the link to my data in the manuscript.

References

Aktar, W., Sengupta, D., Chowdhury, A., 2009. Impact of pesticides use in agriculture: their benefits and hazards. Interdiscip. Toxicol. 2, 1–12. http://dx.doi.org/10.2478/v10102-009-0001-7, URL https://content.sciendo.com/doi/10.2478/v10102-009-0001-7.

Andrade, B.O., Dröse, W., Aguiar, C.A.D., Aires, E.T., Alvares, D.J., Barbieri, R.L., Carvalho, C.J.B.D., Bartz, M., Becker, F.G., Bencke, G.A., Beneduzi, A., Silva, J.B., Blochtein, B., Boldrini, I.I., Boll, P.K., Bordin, J., Silveira, R.M.B.D., Martins, M.B., Bosenbecker, C., Braccini, J., Braun, B., Brito, R., Brown, G.G., Büneker, H.M., Buzatto, C.R., Cavalleri, A., Cechin, S.Z., Colombo, P., Constantino, R., Costa, C.F.D., Dalzochio, M.S., Oliveira, M.G.D., Dias, R.A., Santos, L.A.D., Duarte, A.D.F., Duarte, J.L.P., Durigon, J., Da Silva, M.E., Ferreira, P.P.A., Ferreira, T., Ferrer, J., Ferro, V.G., Fontana, C.S., Freire, M.D., Freitas, T.R.O., Galiano, D., Garcia, M., Dos Santos, T.G., Gomes, L.R.P., Gonzatti, F., Gottschalk, M.S., Graciolli, G., Granada, C.E., Grings, M., Guimarães, P.S., Heydrich, I., Iop, S., Jarenkow, J.A., Jungbluth, P., Käffer, M.I., Kaminski, L.A., Kenne, D.C., Kirst, F.D., Krolow, T.K., Krüger, R.F., Kubiak, B.B., Leal-Zanchet, A.M., Loebmann, D., Lucas, D.B., Lucas, E.M., Luza, A.L., Machado, I.F., Madalozzo, B., Maestri, R., Malabarba, L.R., Maneyro, R., Marinho, M.A.T., Marques, R., Marta, K.D.S., Martins, D.D.S., Martins, G.D.S., Martins, T.R., Mello, A.S.D., Mello, R.L., Mendonça Junior, M.D.S., Morais, A.B.B.D., Moreira, F.F.F., Moreira, L.F.B., Moura, L.D.A., Nervo, M.H., Ott, R., Paludo, P., Passaglia, L.M.P., Périco, E., Petzhold, E.S., Pires, M.M., Poppe, J.L., Quintela, F.M., Raguse-Quadros, M., et al., 2023. 12, 500+ and counting: biodiversity of the Brazilian Pampa. Front. Biogeogr. 15, http://dx.doi.org/10.21425/F5FBG59288, URL https://escholarship.org/uc/item/7tp2k884.

Arocena, R., Castro, M., Chalar, G., 2022. Ecological integrity assessment of streams in the light of natural ecoregions and anthropic land use. Environ. Monit. Assess. 194, 748. http://dx.doi.org/10.1007/s10661-022-10422-z, URL https://link.springer.com/10.1007/s10661-022-10422-z.

Baeza, S., Vélez-Martin, E., De Abelleyra, D., Banchero, S., Gallego, F., Schirmbeck, J., Veron, S., Vallejos, M., Weber, E., Oyarzabal, M., Barbieri, A., Petek, M., Guerra Lara, M., Sarrailhé, S., Baldi, G., Bagnato, C., Bruzzone, L., Ramos, S., Hasenack, H., 2022. Two decades of land cover mapping in the Río de la Plata grassland region: The MapBiomas Pampa initiative. Remote. Sens. Appl.: Soc. Environ. 28, 100834. http://dx.doi.org/10.1016/j.rsase.2022.100834, URL https://linkinghub.elsevier.com/retrieve/pii/S2352938522001422.

Barra, R., Colombo, J.C., Eguren, G., Gamboa, N., Jardim, W.F., Mendoza, G., 2006. Persistent organic pollutants (POPs) in Eastern and Western South American countries. In: Ware, G.W., Nigg, H.N., Doerge, D.R. (Eds.), In: Reviews of Environmental Contamination and Toxicology, vol. 185, Springer New York, New York, NY, pp. 1–33. http://dx.doi.org/10.1007/0-387-30638-2_1, URL http://link.springer.com/10.1007/0-387-30638-2_1.

Boroukhovitch, M., 1998. Uruguay -Current state of chlorine containing pesticides in Uruguay. URL https://www.rapaluruguay.org/sitio_1/lindano/CurrentState.html.

Bruel, R., Sabatier, P., 2020. serac: an R package for ShortlivEd RAdionuclide chronology of recent sediment cores. J. Environ. Radioact. 225, 106449. http://dx.doi.org/10.1016/j.jenvrad.2020.106449, URL https://linkinghub.elsevier.com/retrieve/pii/S0265931X20306950.

Bueno, C., Alves, F., Pinheiro, L., Perez, L., Agostini, V., Fernandes, E., Möller, O., Weschenfelder, J., Pinho, G., Wallner-Kersanach, M., Moura, R., Durán, J., Etchevers, I., Costa, L., Werlang, C., Bortolin, E., Machado, E., Figueira, R., Ferreira, P., Andrade, C., Fornaro, L., García-Rodríguez, F., 2021. The effect of agricultural intensification and water-locking on the world's largest coastal lagoonal system. Sci. Total Environ. 801, 149664. http://dx.doi.org/10.1016/j.scitotenv.2021.149664, URL https://linkinghub.elsevier.com/retrieve/pii/S0048969721047392.

Buishand, T.A., 1982. Some methods for testing the homogeneity of rainfall records. J. Hydrol. 58, 11–27. http://dx.doi.org/10.1016/0022-1694(82)90066-X, URL https://www.sciencedirect.com/science/article/pii/002216948290066X.

Cabernard, L., Pfister, S., Hellweg, S., 2024. Biodiversity impacts of recent land-use change driven by increases in agri-food imports. Nat. Sustain. 7, 1512–1524. http://dx.doi.org/10.1038/s41893-024-01433-4, URL https://www.nature.com/articles/s41893-024-01433-4.

Cabrera, M., Sanabria, R., González, J., Cabral, P., Tejeda, S., Zarazua, G., Melgar-Paniagua, E., Tassano, M., 2023. Using 137Cs and 210Pbex to assess soil redistribution at different temporal scales along with lithogenic radionuclides to evaluate contrasted watersheds in the Uruguayan Pampa grassland. Geoderma 435, 116502. http://dx.doi.org/10.1016/j.geoderma.2023.116502, URL https://linkinghub.elsevier.com/retrieve/pii/S0016706123001799.

Chaboche, P.-A., Pointurier, F., Sabatier, P., Foucher, A., Tiecher, T., Minella, J.P., Tassano, M., Hubert, A., Morera, S., Guédron, S., Ardois, C., Boulet, B., Cossonnet, C., Cabral, P., Cabrera, M., Chalar, G., Evrard, O., 2022. 240Pu/239Pu signatures allow refining the chronology of radionuclide fallout in South America. Sci. Total Environ. 843, 156943. http://dx.doi.org/10.1016/j.scitotenv.2022.156943, URL https://linkinghub.elsevier.com/retrieve/pii/S0048969722040402.

Chamizo, E., García-León, M., Peruchena, J., Cereceda, F., Vidal, V., Pinilla, E., Miró, C., 2011. Presence of plutonium isotopes, 239Pu 240Pu, soils from Chile. Nucl. Instruments Methods Phys. Res. Sect. B: Beam Interactions Mater. Atoms S0168583X11003727, https://linkinghub.elsevier.com/retrieve/pii/S0168583X11003727.

Chiappe, M., Carambula, M., Fernandez, E., 2008. El campo uruguayo: una mirada desde la sociología rural. Montevideo;: Departamento de Publicaciones de la Facultad de Agronomía.

Derpsch, R., Friedrich, T., Kassam, A., Hongwen, L., 2010. Current status of adoption of no-till farming in the world and some of its main benefits. Int. J. Agric. Biological Eng. 3.

Ferreira, P.A.D.L., Figueira, R.C.L., Siegle, E., Asp Neto, N.E., Martins, C.D.C., Schettini, C.A.F., Maciel, P.M., García-Rodriguez, F., Mahiques, M.M.D., 2016. Using a cesium-137 (137 Cs) sedimentary fallout record in the South Atlantic Ocean as a supporting tool for defining the Anthropocene. Anthropocene 14, 34–45. http://dx.doi.org/10.1016/j.ancene.2016.06.002, URL https://linkinghub.elsevier.com/retrieve/pii/S2213305416300510.

Foucher, A., Chaboche, P.-A., Sabatier, P., Evrard, O., 2021. A worldwide meta-analysis (1977–2020) of sediment core dating using fallout radionuclides including ^{137}Cs and ^{210}Pb$_{xs}$. Earth Syst. Sci. Data 13, 4951–4966. http://dx.doi.org/10.5194/essd-13-4951-2021, URL https://essd.copernicus.org/articles/13/4951/2021.

Foucher, A., Tassano, M., Chaboche, P.-A., Chalar, G., Cabrera, M., Gonzalez, J., Cabral, P., Simon, A.-C., Agelou, M., Ramon, R., Tiecher, T., Evrard, O., 2023. Inexorable land degradation due to agriculture expansion in South American Pampa. Nat. Sustain. http://dx.doi.org/10.1038/s41893-023-01074-z, URL https://www.nature.com/articles/s41893-023-01074-z.

Garcia-Préchac, F., Ernst, O., Siri-Prieto, G., Terra, J.A., 2004. Integrating no-till into crop–pasture rotations in Uruguay. Soil Tillage Res. 77, 1–13. http://dx.doi.org/10.1016/j.still.2003.12.002, URL https://linkinghub.elsevier.com/retrieve/pii/S0167198703002514.

Garcia-Rodrıguez, F., Mazzeo, N., Sprechmann, P., Metzeltin, D., Sosa, F., Renom, M., Scharf, B., Gaucher, C., 2002. Paleolimnological assessment of human impacts in Lake Blanca, SE Uruguay. J. Paleolimnol.

Heri, W., Carroll, B., Parshley, T., Nabors, J.B., 2008. Production, development, and registration of triazine herbicides. In: The Triazine Herbicides. Elsevier, pp. 31–43. http://dx.doi.org/10.1016/B978-044451167-6.50006-4, URL https://linkinghub.elsevier.com/retrieve/pii/B9780444511676500064.

Hudson, R.A., Meditz, S.W., Weil, T.E., 1992. Uruguay: a country study, In: Library of Congress (Ed.), second ed. In: Area Handbook Series (Number 550-97), Federal Research Division, Washington, D.C, Library of Congress : For sale by the Supt. of Docs., U.S. G.P.O.

Hurtado, S.I., Zaninelli, P.G., Agosta, E.A., 2020. A multi-breakpoint methodology to detect changes in climatic time series. An application to wet season precipitation in subtropical Argentina. Atmospheric Res. 241, 104955. http://dx.doi.org/10.1016/j.atmosres.2020.104955, URL https://linkinghub.elsevier.com/retrieve/pii/S0169809519315972.

Jeschke, P., Witschel, M., Krämer, W., Schirmer, U. (Eds.), 2019. Modern Crop Protection Compounds, first ed. Wiley, http://dx.doi.org/10.1002/9783527699261, URL https://onlinelibrary.wiley.com/doi/book/10.1002/9783527699261.

Koide, M., Bertine, K.K., Chow, T.J., Goldberg, E.D., 1985. The 240Pu / 239Pu ratio, a potential geochronometer. Earth Planet. Sci. Lett. 72, 1–8. http://dx.doi.org/10.1016/0012-821X(85)90112-8, URL https://linkinghub.elsevier.com/retrieve/pii/0012821X85901128.

Kruk, C., Segura, A., Piñeiro, G., Baldassini, P., Pérez-Becoña, L., García-Rodríguez, F., Perera, G., Piccini, C., 2023. Rise of toxic cyanobacterial blooms is promoted by agricultural intensification in the basin of a large subtropical river of South America. Global Change Biol. 29, 1774–1790. http://dx.doi.org/10.1111/gcb.16587, URL https://onlinelibrary.wiley.com/doi/10.1111/gcb.16587.

Lamb, A.L., Wilson, G.P., Leng, M.J., 2006. A review of coastal palaeoclimate and relative sea-level reconstructions using 13C and C/N ratios in organic material. Earth-Sci. Rev. 75, 29–57. http://dx.doi.org/10.1016/j.earscirev.2005.10.003, URL https://linkinghub.elsevier.com/retrieve/pii/S0012825205001376.

Logan, B.E., Steele, J.A., Arnold, R.G., 1989. Computer simulation of Ddt distribution in Palos verdes shelf sediments. J. Environ. Eng. 115, 221–238. http://dx.doi.org/10.1061/(ASCE)0733-9372(1989)115:1(221), URL https://ascelibrary.org/doi/10.1061/%28ASCE%290733-9372%281989%29115%3A1%28221%29.

Magand, O., Arnaud, F., 2007. Response on the comment from Ribeiro Guevara and Arribere on the article Radionuclide dating (Pb-210, Cs-137, Am-241) of recent lake sediments in a highly geodynamic setting (Lakes Puyehue and Icalma–Chilean lake district). Sci. Total. Environ. 385, 312–314. http://dx.doi.org/10.1016/j.scitotenv.2007.05.022, URL https://linkinghub.elsevier.com/retrieve/pii/S0048969707005463.

Mañay, N., Rampoldi, O., Alvarez, C., Piastra, C., Heller, T., Viapiana, P., Korbut, S., 2004. Pesticides in Uruguay. In: Ware, G.W., Albert, L.A., Crosby, D.G., Voogt, P. De, Hutzinger, O., Knaak, J.B., Mayer, F.L., Morgan, D.P., Park, D.L., Tjeerdema, R.S., Yang, R.S.H., Gunther, F.A. (Eds.), vol. 181, Springer New York, New York, NY, pp. 111–138, URL http://link.springer.com/10.1007/0-387-21733-9_3.

Mellanby, K., 1992. The DDT Story. British Crop Protection Council, Farnham, Surrey, UK.

Merotto, A., Gazziero, D.L.P., Oliveira, M.C., Scursoni, J., Garcia, M.A., Figueroa, R., Turra, G.M., 2022. Herbicide use history and perspective in South America. Adv. Weed Sci. 40, e020220050. http://dx.doi.org/10.51694/AdvWeedSci/2022;40:seventy-five010, URL https://awsjournal.org/article/herbicide-use-history-and-perspective-in-south-america.

Oliveira, T.E.D., Freitas, D.S.D., Gianezini, M., Ruviaro, C.F., Zago, D., Mércio, T.Z., Dias, E.A., Lampert, V.D.N., Barcellos, J.O.J., 2017. Agricultural land use change in the Brazilian Pampa Biome: The reduction of natural grasslands. Land Use Policy 63, 394–400. http://dx.doi.org/10.1016/j.landusepol.2017.02.010, URL https://linkinghub.elsevier.com/retrieve/pii/S0264837716309978.

Overbeck, G., Muller, S., Fidelis, A., Pfadenhauer, J., Pillar, V., Blanco, C., Boldrini, I., Both, R., Forneck, E., 2007. Brazil's neglected biome: The South Brazilian Campos. Perspect. Plant Ecol. Evol. Syst. 9, 101–116. http://dx.doi.org/10.1016/j.ppees.2007.07.005, URL https://linkinghub.elsevier.com/retrieve/pii/S1433831907000303.

Palladino, C., García, I., Fernández, G., 2023. Pesticide dependence and associated risks in Uruguayan agriculture: limitations in its approach. Agrociencia Urug. 27, e1156. http://dx.doi.org/10.31285/AGRO.27.1156, URL https://agrocienciauruguay.uy/index.php/agrociencia/article/view/1156.

Pereira, P.A.A., Martha, G.B., Santana, C.A., Alves, E., 2012. The development of Brazilian agriculture: future technological challenges and opportunities. Agric. & Food Secur. 1, 4. http://dx.doi.org/10.1186/2048-7010-1-4, URL https://agricultureandfoodsecurity.biomedcentral.com/articles/10.1186/2048-7010-1-4.

Perestrelo, R., Silva, P., Porto-Figueira, P., Pereira, J.A., Silva, C., Medina, S., Câmara, J.S., 2019. QuEChERS - Fundamentals, relevant improvements, applications and future trends. Anal. Chim. Acta 1070, 1–28. http://dx.doi.org/10.1016/j.aca.2019.02.036, URL https://linkinghub.elsevier.com/retrieve/pii/S0003267019302259.

Pettitt, A.N., 1979. A non-parametric approach to the change-point problem. J. R. Stat. Soc. Ser. C (Applied Statistics) 28, 126–135. http://dx.doi.org/10.2307/2346729, URL https://www.jstor.org/stable/2346729 Publisher: [Royal Statistical Society, Oxford University Press].

Powell, R.L., Still, C.J., 2009. Biogeography_of_C3_and_C4_vegetation_in_South_Amer.pdf. https://scholar.google.com/scholar?cluster=17252574049958320946&hl=fr&as_sdt=0,5.

Rauh, V., Arunajadai, S., Horton, M., Perera, F., Hoepner, L., Barr, D.B., Whyatt, R., 2011. Seven-year neurodevelopmental scores and prenatal exposure to chlorpyrifos, a common agricultural pesticide. Environ. Heal. Perspect. 119, 1196–1201. http://dx.doi.org/10.1289/ehp.1003160, URL https://ehp.niehs.nih.gov/doi/10.1289/ehp.1003160 Publisher: Environmental Health Perspectives.

Rizzo, G., Monzon, J.P., Ernst, O., 2021. Cropping system-imposed yield gap: Proof of concept on soybean cropping systems in Uruguay. Field Crop. Res. 260, 107944. http://dx.doi.org/10.1016/j.fcr.2020.107944, URL https://linkinghub.elsevier.com/retrieve/pii/S0378429020312284.

Röllin, S., Corcho-Alvarado, J.A., Sahli, H., Putyrskaya, V., Klemt, E., 2022. High-resolution records of cesium, plutonium, americium, uranium isotopes sediment cores from Swiss lakes. Environ. Sci. Pollut. Res. 29, 85777–85788. http://dx.doi.org/10.1007/s11356-022-20785-y, URL https://link.springer.com/10.1007/s11356-022-20785-y.

Severo, O.P., 1955. Eradication of the Aedes Aegypti Mosquito from the Americas. Jefferson History and Publications, URL https://jdc.jefferson.edu/yellow_fever_symposium/6.

Skidmore, M.E., Sims, K.M., Gibbs, H.K., 2023. Agricultural intensification and childhood cancer in Brazil. Proc. Natl. Acad. Sci. 120, e2306003120. http://dx.doi.org/10.1073/pnas.2306003120, URL https://www.pnas.org/doi/10.1073/pnas.2306003120.

Tleuova, A.B., Wielogorska, E., Talluri, V.S.S.L.P., Štěpánek, F., Elliott, C.T., Grigoriev, D.O., 2020. Recent advances and remaining barriers to producing novel formulations of fungicides for safe and sustainable agriculture. J. Control. Release 326, 468–481. http://dx.doi.org/10.1016/j.jconrel.2020.07.035, URL https://www.sciencedirect.com/science/article/pii/S0168365920304193.

Travis, S.C., Aga, D.S., Queirolo, E.I., Olson, J.R., Daleiro, M., Kordas, K., 2020. Catching flame retardants and pesticides in silicone wristbands: Evidence of exposure to current and legacy pollutants in Uruguayan children. Sci. Total Environ. 740, 140136. http://dx.doi.org/10.1016/j.scitotenv.2020.140136, URL https://linkinghub.elsevier.com/retrieve/pii/S0048969720336573.

Turgut, C., Gokbulut, C., Cutright, T.J., 2009. Contents and sources of DDT impurities in dicofol formulations in Turkey. Environ. Sci. Pollut. Res. 16, 214–217. http://dx.doi.org/10.1007/s11356-008-0083-3, URL http://link.springer.com/10.1007/s11356-008-0083-3.

Woodford, E.K., 1957. The toxic action of herbicides. Outlook Agric. 1, 145–154. http://dx.doi.org/10.1177/003072705700100403, URL https://journals.sagepub.com/doi/10.1177/003072705700100403.

Zalles, V., Hansen, M.C., Potapov, P.V., Parker, D., Stehman, S.V., Pickens, A.H., Parente, L.L., Ferreira, L.G., Song, X.-P., Hernandez-Serna, A., Kommareddy, I., 2021. Rapid expansion of human impact on natural land in South America since 1985. Sci. Adv. 7, eabg1620. http://dx.doi.org/10.1126/sciadv.abg1620, URL https://www.science.org/doi/10.1126/sciadv.abg1620.

Zurbriggen, C., González-Lago, M., Baraibar, M., Baethgen, W., Mazzeo, N., Sierra, M., 2020. Experimentation in the design of public policies: The Uruguayan soils conservation plans. Iberoam. – Nord. J. Lat. Am. Caribb. Stud. 49, 52–62. http://dx.doi.org/10.16993/iberoamericana.459, URL http://www.iberoamericana.se/articles/10.16993/iberoamericana.459.